Nicotinamide Prevents UVB- and Oxidative Stress–Induced Photoaging in Human Primary Keratinocytes

JIDOpen

Christina Yan Ru Tan[1,2], Chye Ling Tan[1,2], Toby Chin[1,2], Malgorzata Morenc[1,2], Chin Yee Ho[2,3], Holly A. Rovito[4], Ling Shih Quek[1,2], Ai Ling Soon[2,3], John S.Y. Lim[5], Oliver Dreesen[2,3], John E. Oblong[4] and Sophie Bellanger[1,2]

Nicotinamide (NAM), a NAM adenine dinucleotide precursor, is known for its benefits to skin health. Under standard culture conditions, NAM delays the differentiation and enhances the proliferation of human primary keratinocytes, leading to the maintenance of stem cells. In this study, we investigated the effects of NAM on photoaging in two-dimensional human primary keratinocyte cultures and three-dimensional organotypic epidermal models. In both models, we found that UVB irradiation and hydrogen peroxide induced human primary keratinocyte premature terminal differentiation and senescence. In three-dimensional organotypics, the phenotype was characterized by a thickening of the granular layer expressing filaggrin and loricrin, but thinning of the epidermis overall. NAM limited premature differentiation and ameliorated senescence, as evidenced by the maintenance of lamin B1 levels in both models, with decreased lipofuscin staining and reduced IL-6/IL-8 secretion in three-dimensional models, compared to those in UVB-only controls. In addition, DNA damage observed after irradiation was accompanied by a decline in energy metabolism, whereas both effects were partially prevented by NAM. Our data thus highlight the protective effects of NAM against photoaging and oxidative stress in the human epidermis and pinpoint DNA repair and energy metabolism as crucial underlying mechanisms.

Journal of Investigative Dermatology (2021) ■, ■–■; doi:10.1016/j.jid.2021.10.021

INTRODUCTION

Nicotinamide (NAM), that is, niacinamide or vitamin B_3, is a NAM adenine dinucleotide $(NAD)^+$ precursor with anti-aging properties (Bissett et al., 2005, 2004; Oblong, 2014). We previously showed that NAM promotes human keratinocyte (KC) stem cell maintenance, which may contribute to its beneficial effect on chronological aging (Tan et al., 2019).

In addition to chronological aging, human skin undergoes cumulative damage from daily sun exposure, leading to chronic inflammation, oxidative stress, and photoaging (Yaar and Gilchrest, 2007). Although dermal modifications in both intrinsic and extrinsic aging have been studied extensively, less is known about those in the epidermis (Haydont et al., 2019; Shin et al., 2019). Severe photoaging involves morphological changes that include overall epidermal thinning and flattening of rete ridges with hyperkeratosis, which could be due to reduced desquamation, reduced basal KC proliferation, and stem cell loss (Levakov et al., 2012; López-Otín et al., 2013; Tagami, 2008).

At the molecular level, sunlight induces direct DNA damage and oxidative stress, which in turn amplifies cellular damage through photosensitizing reactions (Rastogi et al., 2010). UVB wavelengths are the main drivers of photoaging in the epidermis (Gilchrest, 2013). This form of irradiation is absorbed by DNA and mediates a direct mutagenic effect through the generation of lesions such as cyclobutane pyrimidine dimers (CPDs) and pyrimidine-(6–4)-pyrimidone photoproducts, eventually causing DNA double-strand breaks (Rastogi et al., 2010; Rünger et al., 2012; Schuch et al., 2017).

UV irradiation induces premature senescence—an irreversible cell cycle arrest controlled by the p53/p21 and/or p16/Rb pathways (Debacq-Chainiaux et al., 2012; Wang et al., 2017). Senescent cells are metabolically active and secrete a range of molecules, including proinflammatory cytokines, chemokines, GFs, and proteases, which collectively constitute the senescence-associated secretory phenotype (SASP) (Coppé et al., 2010). KCs exposed to UVB release SASP factors such as IL-6 and IL-8 (Chung et al., 1996; Kim,

[1]*Stemness, Differentiation, and Aging in the Human Epidermis, A*STAR Skin Research Labs (A*SRL), Agency for Science, Technology and Research (A*STAR), Singapore, Singapore;* [2]*Skin Research Institute of Singapore (SRIS), Singapore, Singapore;* [3]*Cell Aging, A*STAR Skin Research Labs (A*SRL), Agency for Science, Technology and Research (A*STAR), Singapore, Singapore;* [4]*Beauty Technology Division, The Procter & Gamble Company, Mason, Ohio, USA; and* [5]*A*STAR Microscopy Platform, Agency for Science, Technology and Research (A*STAR), Singapore, Singapore*

*Correspondence: Sophie Bellanger, Stemness, Differentiation, and Aging in the Human Epidermis, Skin Research Institute of Singapore (SRIS), A*STAR Skin Research Labs (A*SRL), Agency for Science, Technology and Research (A*STAR), 8A Biomedical Grove, Singapore 138648, Singapore. E-mail: sophie_bellanger@asrl.a-star.edu.sg*

Abbreviations: 2D, two-dimensional; 3D, three-dimensional; CPD, cyclobutane pyrimidine dimer; ECAR, extracellular acidification rate; H_2O_2, hydrogen peroxide; HPK, human primary keratinocyte; K10, keratin 10; KC, keratinocyte; NAD, nicotinamide adenine dinucleotide; NAM, nicotinamide; OCR, oxygen consumption rate; OXPHOS, oxidative phosphorylation; LMNB1, lamin B1; FLG, filaggrin; ROS, reactive oxygen species

Received 14 December 2020; revised 6 October 2021; accepted 19 October 2021; accepted manuscript published online XXX; corrected proof published online XXX

2016; Quist et al., 2016), and senescence was reported 3 days after exposure (Lewis et al., 2008; Wang et al., 2017). However, others failed to detect senescence-associated β-galactosidase–positive cells for up to 12 days after irradiation and instead observed differentiation (de Pedro et al., 2018). Interestingly, late differentiation markers (filaggrin [FLG], loricrin, and involucrin) were induced in human skin 48 hours after UV exposure in a dose-dependent manner (de Pedro et al., 2018; Lee et al., 2002), whereas the mRNA levels of structural proteins from the cornified layer were upregulated 24 hours after irradiation of human foreskin primary KCs (Sesto et al., 2002). In contrast, some studies showed loricrin and FLG downregulation in three-dimensional (3D) organotypic cultures 2−3 days after irradiation (Bernerd and Asselineau, 1997).

The reliance of differentiated versus proliferating human primary KCs (HPKs) on glycolysis or oxidative phosphorylation (OXPHOS), in addition to the possible existence of a switch in energy metabolism that induces differentiation/senescence, remain to be clarified. We previously showed that the shutdown of glycolysis associated with a moderate decline in OXPHOS drives both HPK differentiation and senescence (Tan et al., 2019). This could be linked to increased reactive oxygen species (ROS) production since mitochondrial ROS generation through OXPHOS modulation was reported to promote differentiation of KC stem cells (Hamanaka et al., 2013; Hornig-Do et al., 2007; Lago et al., 2012; Tamiji et al., 2005). However, OXPHOS modulation can induce KC senescence and differentiation independent of ROS generation (Wiley et al., 2016).

In this study, we used both two-dimensional (2D) cultures and 3D organotypic epidermal models to show that NAM facilitates DNA repair while maintaining energy metabolism, thereby preventing the onset of accelerated differentiation and premature senescence in HPKs exposed to UVB or oxidative stress. Our findings provide further mechanistic insights into the antiphotoaging properties of NAM.

RESULTS

NAM prevents premature late differentiation induced by UVB in both 3D organotypics and 2D HPK cultures

After exposure of mature 3D organotypic epidermal cultures to 25 mJ/cm^2 UVB, Ki-67 and keratin 10 (K10) protein expression levels were unaltered (Figure 1a). In contrast, the levels of FLG and loricrin increased, with the thickening of the upper granular layers expressing these two proteins. NAM treatment prevented this phenomenon, thus preserving the overall epidermal structure of the epithelium. When the UVB dose was increased, we observed overall epidermal thinning that was severe at 200 mJ/cm^2 (Supplementary Figure S1a). Loricrin and FLG were expressed in >50% of the epithelium, although K10 was expressed by fewer layers and was almost absent from the suprabasal/spinous layers, indicating premature late differentiation. Although NAM did not restore normal epidermal thickness, it partially prevented late differentiation and improved overall epidermal structure.

In accordance with our 3D findings, late differentiation markers were induced in 2D cultures 3 days after UVB irradiation at 25 mJ/cm^2, and incubation with NAM for 1 day or 3 days inhibited their expression at the protein and mRNA levels in a time-dependent manner (Figure 1b–d and Supplementary Figure S1b). After 3 days of NAM treatment, we observed 30−90% inhibition depending on the experiments/markers tested. Interestingly, although we detected no significant decrease in the expression of Ki-67 in the 3D organotypics after UVB irradiation (Supplementary Figure S2a and b), 25 mJ/cm^2 resulted in an almost complete cessation of HPK proliferation in 2D cultures and a loss of Ki-67, which was partially prevented by NAM treatment in a time-dependent manner. However, NAM-treated cells, including Ki-67–positive cells, still appeared larger and flatter after irradiation than the control cells (Figure 1b and Supplementary Figure S1b).

NAM prevents senescence after UVB irradiation in both 3D and 2D HPK cultures

To investigate the ability of NAM to protect HPKs against premature senescence after UVB irradiation, we exposed organotypic cultures to high (50−200 mJ/cm^2) or low (25−50 mJ/cm^2) doses of UVB (Figure 2 and Supplementary Figure S3, respectively). In the absence of UVB irradiation, lamin B1 (LMNB1) levels, known to decrease in senescent cells (Dreesen et al., 2013), were approximately two-fold higher in the basal layer (K10-negative) than in the suprabasal/upper layers (K10-positive), suggesting that senescence normally occurs in the upper differentiated layers (Figure 2a and b and Supplementary Figure S3a and b). After high-dose UVB irradiation (Figure 2), a decline in LMNB1 levels occurred in all layers, consistently significant in the upper layers but only significant at doses >50 mJ/cm^2 in the basal layer. Importantly, NAM treatment maintained LMNB1 expression in all layers for doses up to 100 mJ/cm^2 (Figure 2a and b). When the dose was reduced to 25 or 37 mJ/cm^2, no significant changes in LMNB1 levels were detected in any layer compared with the levels expressed in the absence of UVB irradiation (Supplementary Figure S3a and b). Although not significant, there was a slight decline in LMNB1 at 50 mJ/cm^2 in both the lower and upper layers, indicating that 50 mJ/cm^2 may be the threshold dose required to detect senescence in 3D organotypic cultures. Nonetheless, LMNB1 levels were consistently and significantly higher in the UVB + NAM population than in the corresponding UVB population for all low doses and unexpectedly higher than in the nonirradiated population (Supplementary Figure S3a and b). Interestingly, because NAM did not increase LMNB1 expression in the nonirradiated cells, the positive effect of NAM seemed to be specific to stressed cells, as previously proposed (Tan et al., 2019). For all high and low doses, the total number of cells per field throughout the whole epithelium was significantly reduced by irradiation, and NAM partially prevented this decrease at UVB doses up to 100 mJ/cm^2 (Figure 2c and Supplementary Figure S3c).

Inhibition of senescence by NAM in 3D models was confirmed by SenTraGor (GL13) labeling of lipofuscin, a recently described senescence biomarker that stains aggregates composed of highly oxidized molecules (Supplementary Figure S4, arrows). Positively stained brown

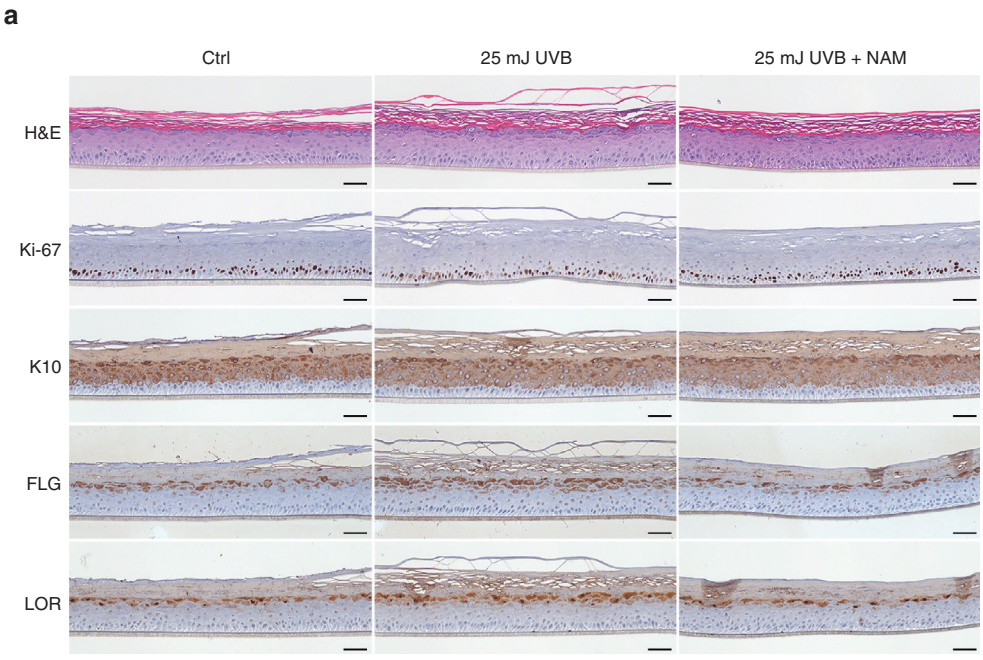

Figure 1. NAM prevents premature late differentiation induced by UVB in both 3D organotypics and 2D cultures of HPKs. (**a**) H&E staining and immunohistochemistry analyses of full-thickness epithelia treated as indicated. Bar = 50 μm. (**b**) Immunofluorescence analyses (Ki-67, red; FLG, green; DAPI, blue) performed on day 3 after treating HPKs (2D cultures) as indicated. Bar = 50 μm. (**c**) Western blot analyses after treating HPKs as in **b**. (**d**) RT-qPCR analyses after treating HPKs as in **b**. Statistical analyses: paired *t*-tests, n = 4–12, *P*-values < 0.05 indicate statistical significance (*$P < 0.05$; **$P < 0.01$; ***$P < 0.001$). 2D, two-dimensional; 3D, three-dimensional; Ctrl, untreated control cells; FLG, filaggrin; HPK, human primary keratinocyte; IVL, involucrin; K10, keratin 10; LOR, loricrin; NAM, nicotinamide; n.s., not significant.

granules were present in UVB-irradiated HPKs, and a protective effect of NAM was detected at both 100 and 200 mJ/cm^2. In addition, the senescence-associated secretory phenotype proteins IL-6 and IL-8 accumulated in the medium after 100 mJ/cm^2 UVB, peaking at 24 hours before the levels started to decline. NAM efficiently mitigated their secretion, with a reduction to basal levels of IL-6 after 48 hours and a 30% reduction in IL-8 levels (Figure 2d).

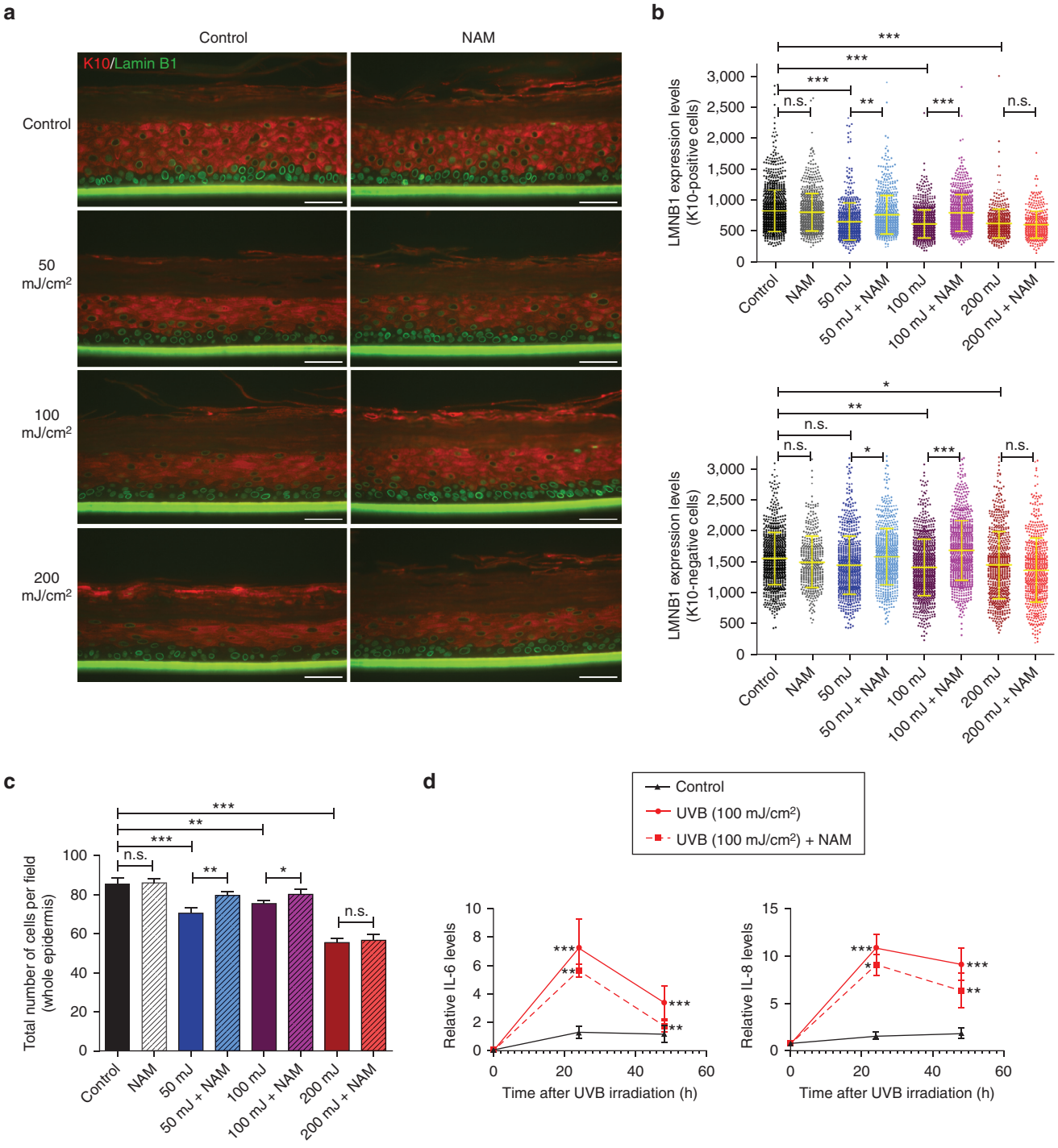

Figure 2. NAM prevents senescence after UVB irradiation in 3D organotypics. (**a**) Immunofluorescence analyses of full-thickness epithelia treated as indicated. Bar = 50 μm. (**b**) Lower and upper panels show LMNB1 levels per cell in K10-negative (basal layer) and K10-positive (suprabasal and upper layers) cells, respectively. Each dot represents one cell. A total of 450−1,100 cells per condition (from triplicates) were analyzed. Statistical analyses: unpaired *t*-tests. Bar = 50 μm. (**c**) Total numbers of cells per field (according to DAPI staining): 19−25 fields per condition (from triplicates). Statistical analyses: unpaired *t*-tests. (**d**) Relative levels of IL-6 and IL-8 24 and 48 h after UVB irradiation (100 mJ/cm^2) detected by ELISA. Statistical analyses: two-way ANOVA, n = 5−6. For all panels, *P*-values < 0.05 indicate statistical significance (*$P < 0.05$; **$P < 0.01$; ***$P < 0.001$). 3D, three-dimensional; h, hour; K10, keratin 10; LMNB1, lamin B1; NAM, nicotinamide; n.s., not significant.

In contrast to 3D organotypics, immunofluorescence analysis revealed a dramatic reduction in LMNB1 levels in 2D models 3 days after UVB irradiation at the lowest dose (25 mJ/cm^2), indicating extensive senescence concomitant with differentiation (Figure 3a and Supplementary Figure S5a). Senescence was confirmed by an increase in p21 levels and the loss of Ki-67 (Figure 3a and b and Supplementary Figure S5a and b). Immunofluorescence also showed that NAM treatment for both 1 day and 3 days partially prevented senescence in a time-dependent manner (Figure 3a and b and

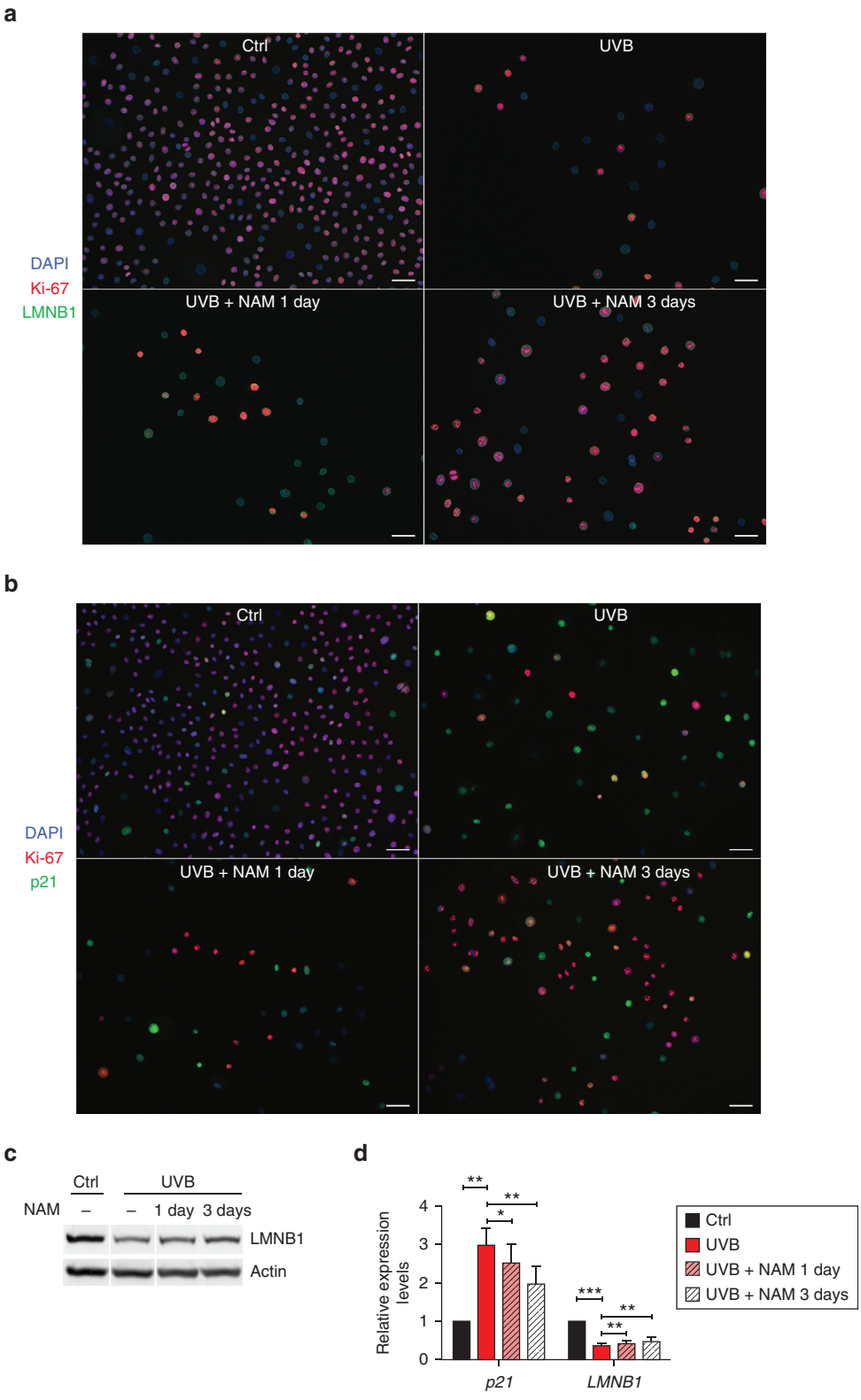

Figure 3. NAM prevents senescence after UVB irradiation in 2D cultures of HPKs. (**a**) Immunofluorescence analyses (Ki-67, red; LMNB1, green; DAPI, blue) on day 3 after treating HPKs (2D cultures) as indicated. Bar = 50 μm. (**b**) Immunofluorescence analyses (Ki-67, red; p21, green; DAPI, blue) in HPKs treated as in **a**. Bar = 50 μm. (**c**) Western blot analyses after treating HPKs as in **a**. (**d**) RT-qPCR analyses after treatment of HPKs as in **a**. Statistical analyses: paired *t*-test, n = 4–9 depending on conditions, *P*-values < 0.05 indicate statistical significance (*$P < 0.05$; **$P < 0.01$; ***$P < 0.001$). 2D, two-dimensional; Ctrl, untreated control cell; HPK, human primary keratinocyte; LMNB1, lamin B1; NAM, nicotinamide.

Supplementary Figure S5a and b), which was confirmed by western blot (Figure 3c), RT-qPCR (Figure 3d), and senescence-associated β-galactosidase activity profiling (Supplementary Figure S6a). Overall, NAM prevented UVB-induced senescence by up to a maximum of 50% in 2D models depending on the senescence marker used.

Hydrogen peroxide treatment mimics UVB exposure in 2D and 3D HPK cultures, and the effects can be prevented by NAM

Because UV irradiation leads to a significant increase in peroxide levels as part of the oxidative stress response (D'Orazio et al., 2013), we examined the ability of hydrogen

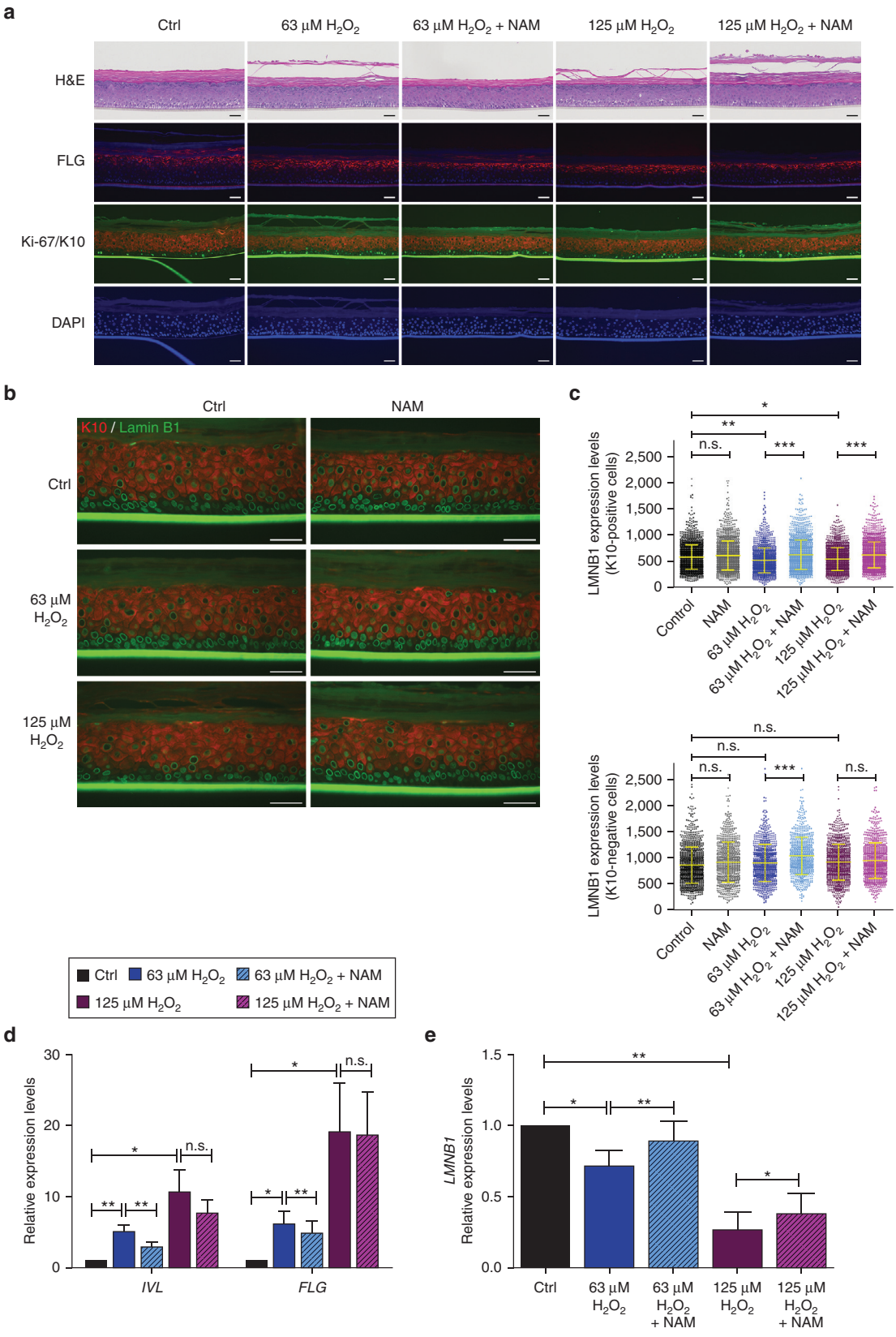

Figure 4. H_2O_2 treatment mimics UVB exposure, inducing both late differentiation and senescence, which were prevented by NAM, in 2D and 3D cultures of HPKs. (**a**) H&E staining and immunofluorescence analyses of full-thickness epithelia. Bar = 50 μm. (**b**) Immunofluorescence analyses performed as in **a**. Bar = 50 μm. (**c**) Lower and upper panels show LMNB1 levels per cell in K10-negative (basal layer) and K10-positive (suprabasal and upper layers) cells, respectively. Each dot represents one cell. A total of 900–1,800 cells were analyzed (from triplicates). Statistical analyses: unpaired *t*-tests. Bar = 50 μm. (**d, e**) RT-qPCR from HPKs (2D) treated as indicated. Statistical analyses: paired *t*-test, n = 5–6. For all panels, *P*-values < 0.05 indicate statistical significance (*$P < 0.05$; **$P < 0.01$;

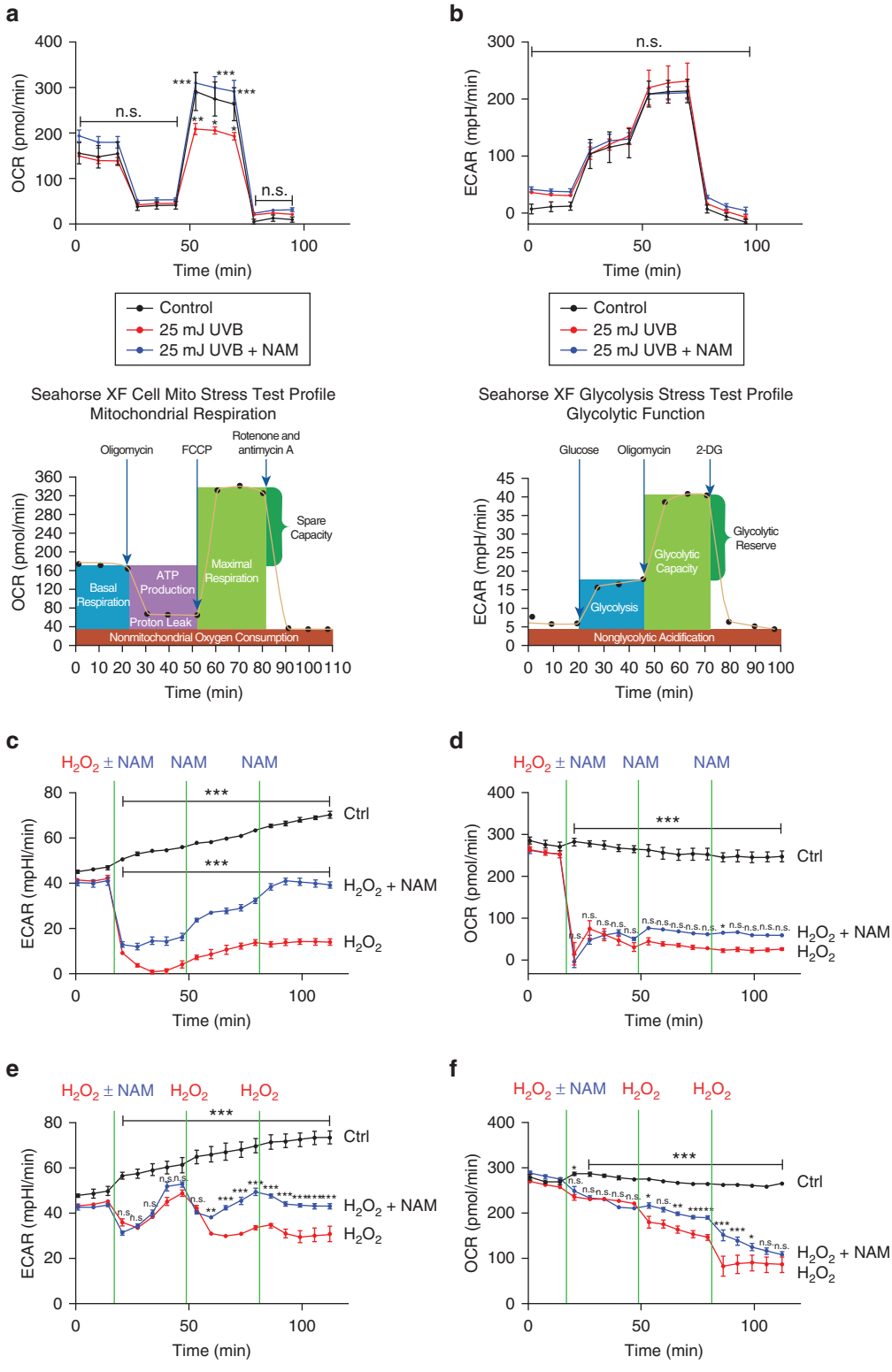

Figure 5. NAM rescues energy metabolism defects caused by UVB and H_2O_2. (**a**) OCR (OXPHOS) measurements in HPKs treated as indicated. (**b**) ECAR (glycolysis) measurements in cells treated as in (**a**). Upper panel: experimental results. Lower panel: the protocol used and parameters measured. (**c**) Basal ECAR levels in HPKs treated as indicated. (**d**) Basal OCR levels in HPKs treated as in **c**. (**e**) Basal ECAR levels in HPKs treated as indicated. (**f**) Basal OCR levels in HPKs treated as in **e**. In all cases, statistical analyses were performed by two-way ANOVA, n = 3 for **a–d** or n = 5 for **e** and **f**. For all panels, *P*-values < 0.05 indicate statistical significance (*$P < 0.05$; **$P < 0.01$; ***$P < 0.001$). 2-DG, 2-deoxyglucose; ATP, adenosine triphosphate; Ctrl, control; ECAR, extracellular acidification rate; FCCP, trifluoromethoxy carbonylcyanide phenylhydrazone; H_2O_2, hydrogen peroxide; HPK, human primary keratinocyte; min, minute; NAM, nicotinamide; n.s., not significant; OCR, oxygen consumption rate; OXPHOS, oxidative phosphorylation.

peroxide (H_2O_2) (a ROS precursor) treatment to mimic the HPK phenotype induced by UVB irradiation (Figure 4). Epidermal thinning was observed in 3D cultures treated with H_2O_2 at both 63 and 125 μM. Although the granular layer expressing FLG seemed only slightly thicker than the control, the overall thinning led to this layer now occupying approximately 50% of the epithelium. Strikingly, this was reminiscent of what we observed after high UVB exposure and was ameliorated by NAM treatment (Figure 4a). Consistent with the UVB findings in 3D, H_2O_2 did not affect

***$P < 0.001$). 2D, two-dimensional; 3D, three-dimensional; Ctrl, untreated control cell; FLG, filaggrin; H_2O_2, hydrogen peroxide; HPK, human primary keratinocyte; IVL, involucrin; K10, keratin 10; LMNB1, lamin B1; NAM, nicotinamide; n.s., not significant.

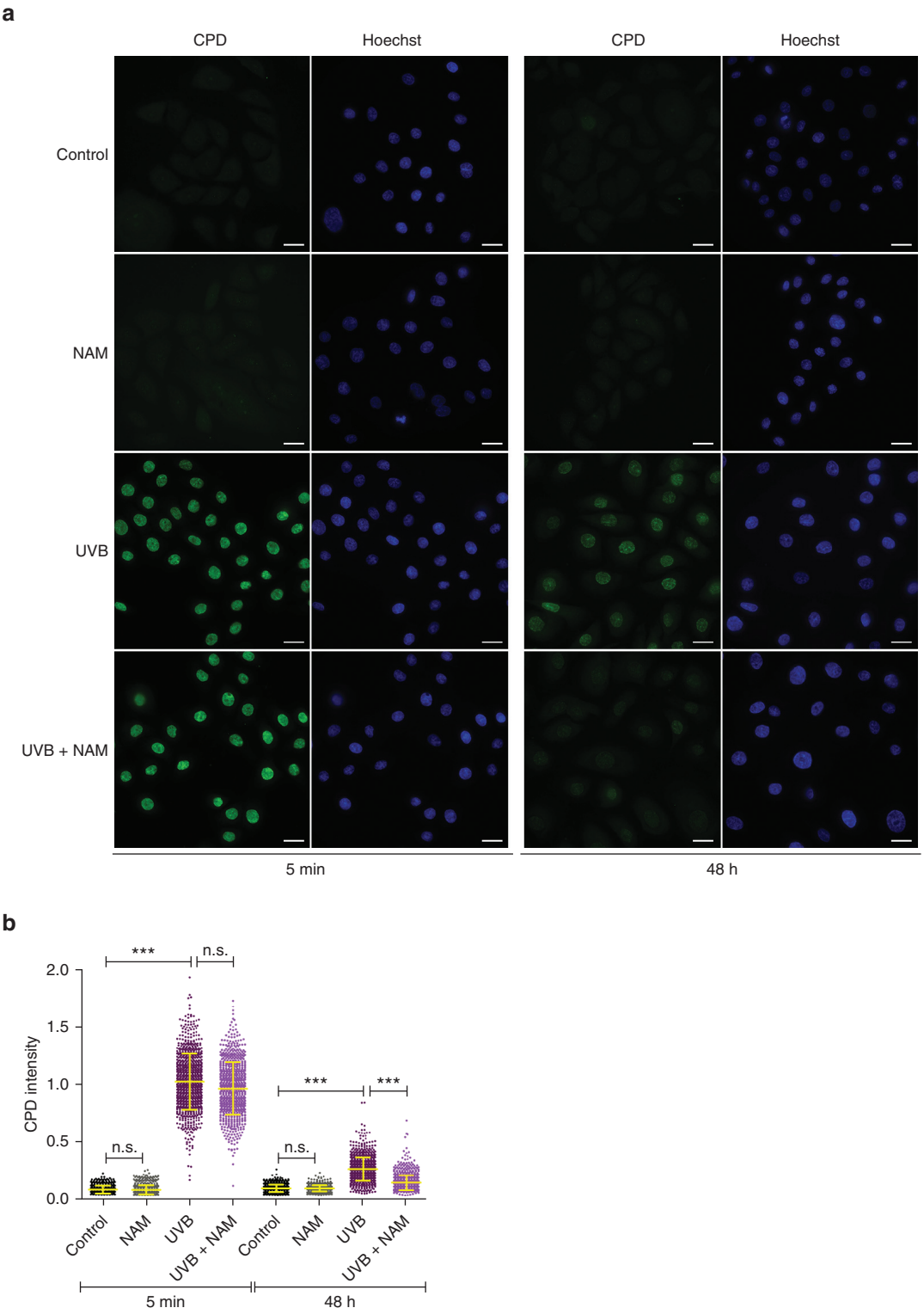

Figure 6. NAM improves DNA repair after UVB irradiation (25 mJ/cm^2). (**a**) Immunofluorescence analyses showing CPD staining in HPKs treated as indicated. Bar = 25 μm. (**b**) Quantification of CPD intensity per cell. Each dot represents one cell. A total of 700−1,800 cells were analyzed (from triplicates). Statistical analyses: unpaired *t*-tests. *P*-values < 0.05 indicate statistical significance (***$P < 0.001$). CPD, cyclobutane pyrimidine dimer; h, hour; HPK, human primary keratinocyte; min, minute; NAM, nicotinamide; n.s., not significant.

the Ki-67 staining in the basal layer (Supplementary Figure S7).

As observed after low-dose UVB irradiation, H_2O_2 had no significant effect on LMNB1 expression in the basal layer (Figure 4b and c). However, treatment with 63 μM H_2O_2 and NAM led to significantly higher LMNB1 levels than those in cells treated with H_2O_2 alone (and in control cells), which was similar to the phenotype observed after low-dose UVB irradiation and NAM treatment. For both concentrations, H_2O_2 treatment resulted in significantly reduced LMNB1 levels in the

upper layers, which was efficiently prevented by NAM, thus reproducing the phenotype observed after treatment with 100 mJ/cm^2 UVB. Senescence was confirmed by increased lipofuscin staining, and as observed for the reduction in LMNB1 expression in the upper layers, the H_2O_2-induced lipofuscin signal was prevented by NAM (Supplementary Figure S8).

RNA analysis of the 2D cultures showed strong dose-dependent induction of *FLG* and *involucrin* 5 days after H_2O_2 treatment, which was significantly inhibited by NAM after 63 μM H_2O_2, whereas the effect was only partial after 125 μM H_2O_2 (Figure 4d). The dose-dependent induction of senescence by H_2O_2 was indicated by the reduction in *LMNB1* mRNA levels (Figure 4e) and increased senescence-associated β-galactosidase activity (Supplementary Figure S6b), which were partially prevented by NAM treatment.

NAM rescues energy metabolism defects caused by UVB and H_2O_2

We then investigated the ability of UVB to modulate cellular metabolism and the potential protective effects of NAM. To this end, we measured OXPHOS (oxygen consumption rate [OCR]) and glycolysis (extracellular acidification rate [ECAR]) in real time 24 hours after UVB irradiation using a Seahorse Analyzer (Agilent, Santa Clara, CA) (Figure 5). Although basal respiration was not significantly modulated by UVB, we observed a reduction in the spare respiratory capacity, which was restored by NAM (Figure 5a). In contrast, glycolysis levels were unchanged and were unaffected by NAM treatment (Figure 5b).

H_2O_2 is known to provoke a decrease in both OXPHOS and glycolysis by shifting energy metabolism toward the oxidative pentose phosphate pathway to generate the ROS scavenger NAM adenine dinucleotide phosphate (NADPH) (Kuehne et al., 2015). As expected, H_2O_2 alone provoked a decline in both glycolysis and OXPHOS, and the cells did not recover over the 2-hour duration of the experiment (Figure 5c and d). Coinjection of NAM with H_2O_2 followed by two additional NAM injections 30 minutes and 1 hour later resulted in a similar initial metabolic decrease, but glycolysis recovered in a NAM dose-dependent manner, reaching approximately 50% of the initial basal activity at the highest NAM dose (Figure 5c and Supplementary Figure S9). Similarly, coinjecting NAM with H_2O_2 followed by two additional H_2O_2 injections efficiently protected glycolysis after the second and third H_2O_2 injections (Figure 5e). Interestingly, NAM mediated only a modest effect in preventing the OXPHOS decline, with no significant effect observed with the first protocol, although the OCR of the cells treated with H_2O_2 + NAM was consistently higher than that of the cells treated with H_2O_2 alone (Figure 5d). Using the second protocol, NAM significantly delayed the decrease in OXPHOS after the second and third H_2O_2 injections but not beyond 100 minutes (Figure 5f).

NAM improves DNA repair in 2D HPK cultures after UVB irradiation

Because both adenosine triphosphate (ATP) and NAD^+ are essential for the activity of DNA repair enzymes such as poly(ADP-ribose) polymerase (PARP), chromatin remodelers, or DNA ligases, NAM may indirectly enhance the DNA damage response under photoaging conditions (Chung and Joe, 2014; Ke et al., 2019; Luna et al., 2013; Osley et al., 2007). As expected, CPD staining in 2D cultures increased immediately after UVB irradiation, indicating DNA lesions (Figure 6a). Remarkably, although CPDs were partially resolved in control cells after 48 hours (74% reduction for the UVB sample), evidence that DNA repair was significantly enhanced by NAM was obtained by the further decline in CPD levels, reaching an overall reduction of 85% (Figure 6b). These results show that NAM treatment increased the efficiency of DNA repair after UVB exposure.

DISCUSSION

In this study, we show that HPK differentiation and senescence are induced by UVB and H_2O_2 in 2D cultures and 3D organotypics and that these phenotypes can be partially prevented by NAM treatment. Furthermore, we show that this prevention occurs by maintaining energy metabolism and enhancing DNA repair. Thus, our findings indicate the potential of NAM as a powerful agent that can protect against photoaging.

We observed that only UVB doses ≥50 mJ/cm^2 induced a significant loss of LMNB1 in 3D organotypics, whereas 25 mJ/cm^2 was sufficient in 2D cultures. Therefore, it is conceivable that acute UVB irradiation ≤50 mJ/cm^2 fails to induce senescence in the epidermis, although it is sufficient to promote premature differentiation. Nevertheless, we do not favor this hypothesis because all samples exposed to low-dose irradiation and treated with NAM still showed a significant increase in LMNB1 in both the basal and upper layers. This increase was inversely proportional to the dose of UVB (Supplementary Figure S3). Interestingly, we observed the same phenomenon in the basal layer after cotreatment with 63 μM H_2O_2 and NAM. Interpretation of this finding is complex; we propose that senescence is induced in the 3D organotypics after UVB exposure at all doses, although the associated reduction in LMNB1 expression could be counterbalanced by an increase in LMNB1 driven by another unidentified mechanism concomitantly activated by irradiation. This pathway would compensate for the loss of LMNB1 after low-dose UVB irradiation but not after high-dose exposure (because the senescence rate would be higher in this case). Cotreatment with NAM would then prevent the reduction in LMNB1 levels induced by high UVB doses, whereas it would increase LMNB1 levels compared with that in nonirradiated cells after low UVB doses. Of note, 200 mJ/cm^2 UVB irradiation induced dramatic senescence that could no longer be prevented by NAM treatment. The decline in LMNB1 after UVB exposure in the absence of NAM was more pronounced in the upper layers (30% decrease) than in the basal layers (10% decrease); similarly, H_2O_2 affected the LMNB1 levels only in the upper layers. We hypothesize that basal cells, including stem cells, preferentially respond to stress by premature differentiation instead of senescence, whereas differentiated cells are more prone to senescence.

Although the energy pathway affected (OXPHOS or glycolysis) may differ depending on the type of stress applied to the epidermis, we show that energy metabolism decreases after UVB or oxidative stress. We propose that this decline, which can be prevented by NAM, drives the loss of stem cells through premature differentiation and senescence. In support

of our findings that NAM exerts protective effects against photoaging, we further found that DNA damage repair in HPKs was enhanced by NAM, corroborating previous reports of similar effects in other cell types (Fania et al., 2019; Surjana et al., 2010). This evidence highlights a dual protective role of NAM against both DNA damage and the decline in energy metabolism associated with photoaging conditions.

Both DNA repair and metabolism require NAD^+, and we show in this study that the maximal OXPHOS capacity is reduced after UVB irradiation, possibly owing to the diversion of NAD^+ to the DNA repair pathway. We propose that increasing the NAD^+ pool through NAM complementation permits more flexibility after irradiation by allowing cells to repair DNA without dramatically affecting energy metabolism. In addition, maintaining energy metabolism will ultimately help to maintain adenosine triphosphate–dependent DNA repair. We also observed limited secretion of the senescence-associated secretory phenotype components IL-6 and IL-8 in UVB-irradiated HPKs treated with NAM, probably owing to fewer cells undergoing senescence. Interestingly, IL-6 secretion is correlated with UV-induced CPD formation (Chung et al., 1996), whereas IL-8 exacerbates DNA damage through increased ROS production (Alexander et al., 2013). Therefore, the maintenance of low levels of these ILs by NAM could also participate in limiting DNA damage.

Remarkably, these effects of NAM might explain its preventive role in the occurrence of nonmelanoma skin cancers known to be induced by UVR (Chen et al., 2015; Kim et al., 2015). As such, our findings should be considered in terms of the potential value of NAM for improving the capacity to prevent and treat clinical skin conditions linked to sun exposure (e.g., actinic keratosis and basal/squamous cell carcinomas) and for developing cosmetic applications targeting stress-induced skin aging.

MATERIALS AND METHODS

Study approval

This study was approved by the National University of Singapore Institutional Review Board (National University of Singapore Institutional Review Board reference code B-14-257E) and the Agency for Science Technology and Research Institutional Review Board (Institutional Review Board references 2019-053 and 2021-082).

Primary KC isolation from human skin

HPKs were obtained and isolated as previously described (Quek et al., 2018) from healthy human skin samples (upper limb of a donor aged 41 years and foreskin from donors aged 6 years) from deidentified surplus surgical waste with written informed patient consent and ethical clearance.

HPK 2D culture and UVB irradiation/H_2O_2 treatment

For maintenance, HPKs were cultured on lethally irradiated murine 3T3-J2 feeder cells as previously described (Rheinwald and Green, 1975; Simon and Green, 1985; Tan et al., 2019).

One day before irradiation/H_2O_2 treatment, HPKs were seeded into a feeder-free system in Dermalife medium (LL-0007; Lifeline Cell Technology, Oceanside, CA). The medium was changed (±NAM) just before the cells were irradiated with UVB using the BioSun system (Vilber, Collégien, France). The medium was replaced immediately after irradiation to ±NAM medium. For H_2O_2 treatment, cells were treated with H_2O_2 (±NAM) for 30 minutes before the medium was changed to ±NAM medium.

RT-qPCR

Total mRNA was extracted and reverse transcribed, and RT-qPCR analysis was carried out as previously described (Thierry et al., 2004) using the primer sequences listed in Supplementary Table S1.

Immunofluorescence analysis

HPKs were fixed and permeabilized with ice-cold acetone/methanol (1:1) for 7 minutes at −20 °C or with 4% paraformaldehyde followed by Triton/PBS depending on the antibody used, and blocked with PBS/2% serum. They were incubated with primary antibodies (Supplementary Table S2) followed by secondary antibodies (Alexa Fluor 488 or 568, Invitrogen, Carlsbad, CA) and DAPI (Sigma-Aldrich, Saint-Louis, MO) before mounting with Hydromount (Electron Microscopy Sciences, Hatfield, PA). Images were captured with a Zeiss AxioImager Z1 microscope and analyzed using Zen 2 software (Zeiss, Oberkochen, Germany).

For CPD labeling, cells were fixed in paraformaldehyde as described earlier, treated with 2 M hydrogen chloride for 30 minutes, and blocked with 20% fetal bovine serum followed by a 30-minute incubation with anti-CPD antibody (Supplementary Table S2) at 37 °C. Secondary detection was achieved with an Alexa Fluor 488 antibody (Invitrogen), and Hoechst was used as a nuclear dye. Coverslips were mounted onto slides using ProLong Diamond Antifade Mountant (ThermoFisher Scientific, Waltham, MA), and images were acquired on an IX-83 Olympus microscope.

CPD quantification

Nuclei segmentation was performed using the threshold function, and the mean intensity of the CPD fluorescence was measured with ImageJ (version 1.52o; National Institutes of Health, Bethesda, MD). For each experiment, CPD fluorescence intensity was normalized to the mean intensity 5 minutes after UVB.

Glycolysis and OXPHOS measurement

As measures of the rates of OXPHOS and glycolysis, respectively, the OCR and ECAR were determined using the Seahorse XFe 24 Analyzer (Agilent).

For UVB experiments, HPKs were seeded into an XF24 microplate (Agilent) 24 hours before irradiation (25 mJ/cm^2 UVB). After 24 hours, the medium was replaced with a custom-made EpiLife medium (Life Technologies, Carlsbad, CA), and cells were treated as previously described (Tan et al., 2019). The Seahorse XF Cell Mito Stress Test Kit (103015-100, Agilent) and Seahorse XF Glycolysis Stress Test Kit (103020-100, Agilent) were used according to the manufacturer's instructions. The OCR was based on three basal measurements, repeated after injection of oligomycin (1 μM), trifluoromethoxy carbonylcyanide phenylhydrazone (1 μM), and rotenone/antimycin A (0.5 μM). The ECAR was based on three basal measurements, repeated after injection of glucose (10 mM), oligomycin (1 μM), and 2-deoxyglucose (50 mM).

To quantify the OCR and ECAR after H_2O_2/NAM treatments, HPKs were seeded 1 day before analysis. The basal OCR and ECAR were measured before and after a series of injections (using the ports): (i) H_2O_2 (1.5 mM) coinjected with NAM (0.25, 0.5, or 1 mM), followed by two injections of NAM (0.25, 0.5, or 1 mM) 30 minutes and 1 hour later, respectively; or (ii) H_2O_2 (0.5 mM) coinjected with NAM (1.5 mM) followed by two injections of H_2O_2 (0.5 mM) 30 minutes and 1 hour later, respectively. Raw OCR and ECAR values were

normalized to the viable cell number using crystal violet staining (C3886, Sigma-Aldrich) as previously described (Tan et al., 2019).

Protein extraction and western blotting

Protein extraction and western blotting were performed as previously described (Quek et al., 2018) using the antibodies listed in Supplementary Table S2.

3D organotypic skin epidermis culture

Human epidermis models (3D NHEK for H_2O_2 experiments or EPI-200-3S-D2 for UVB experiments; MatTek Corporation, Ashland, MA) derived from the newborn foreskin were used according to the manufacturer's instructions. Tissues were pretreated with 1.5 mM NAM for 16 hours before UVB or H_2O_2 treatment. The medium was replaced every 2 days; the tissues were harvested on day 6 after treatment, fixed in 10% neutral buffered formalin for 4 hours, and embedded in paraffin blocks.

Immunohistochemistry analysis of 3D organotypic sections

Immunohistochemistry analysis of paraffin-embedded sections was performed using specific primary antibodies (Supplementary Table S2) as previously described (Tan et al., 2019).

Immunofluorescent staining of 3D organotypic sections

Paraffin-embedded tissue sections were prepared as described by Tan et al. (2019) but without H_2O_2 treatment. Sections were exposed to primary antibodies for 1 hour followed by a 30-minute incubation with secondary antibodies (Alexa Fluor 488 or 568, Invitrogen) and 10-minute incubation with DAPI (Sigma-Aldrich) before mounting with Hydromount (Electron Microscopy Sciences).

LMNB1 quantification

Images were acquired on the Zeiss AxioImager Z1 using a ×40 plan apochromatic objective lens. Perinuclear LMNB1 expression levels were determined using ImageJ, version 1.52o, with a self-written algorithm (Supplementary Materials and Methods). K10 staining was used to visualize the basal (K10-negative) versus suprabasal (K10-positive) layers.

ELISA

Supernatants from 3D organotypics were collected 24 and 48 hours after irradiation. ELISAs were performed according to the manufacturer's instructions (antibodies are listed in Supplementary Table S2) using a microplate reader (Spark, Tecan, Männedorf, Switzerland). Quantitative analysis of samples was performed using a Four Parameter Logistic curve fit.

Statistical analyses

Statistical analyses were performed using GraphPad Prism, version 5.03 (GraphPad Software, San Diego, CA), with one-way ANOVA, two-way ANOVA, or *t*-test as indicated. $P < 0.05$ indicates statistical significance (*$P < 0.05$, **$P < 0.01$, ***$P < 0.001$; n.s., not significant). All data represent the means ± SEM, except for LMNB1 and CPD quantifications, where data represent the means ± SD.

Data availability statement

No datasets were generated or analyzed during this study.

ORCIDs

Christina Yan Ru Tan: http://orcid.org/0000-0003-1901-5934
Chye Ling Tan: http://orcid.org/0000-0001-7688-1316
Toby Chin: http://orcid.org/0000-0003-0025-7992
Malgorzata Morenc: http://orcid.org/0000-0001-8467-6283
Chin Yee Ho: http://orcid.org/0000-0001-7413-4288
Holly A. Rovito: http://orcid.org/0000-0003-2352-1477
Ling Shih Quek: http://orcid.org/0000-0002-3861-8901
Ai Ling Soon: http://orcid.org/0000-0003-3349-1689
John S.Y. Lim: http://orcid.org/0000-0001-9837-6644
Oliver Dreesen: http://orcid.org/0000-0003-1148-3557
John E. Oblong: http://orcid.org/0000-0001-7628-6242
Sophie Bellanger: http://orcid.org/0000-0002-0689-2201

CONFLICT OF INTEREST

JEO and HAR are full-time employees of The Procter & Gamble Company (Cincinnati, OH). The remaining authors state no conflict of interest.

ACKNOWLEDGMENTS

The authors would like to thank the Asian Skin Bioank for supplying the human primary keratinocyte cells and Jessica Tamanini of Insight Editing London for English language editing of this manuscript. This study was supported by the Agency for Science, Technology and Research (A*STAR) and The Procter & Gamble Company.

AUTHOR CONTRIBUTIONS

Conceptualization: SB, JEO; Data Curation: SB; Formal Analysis: CYRT, CLT, TC, MM, CYH, ALS, SB; Funding Acquisition: SB, JEO; Investigation: CYRT, CLT, TC, MM, CYH, LSQ, ALS; Methodology: CYRT, CLT, TC, MM, CYH, HAR; Project Administration: SB, JEO; Resources: TC, LSQ; Software: JSYL; Supervision: SB, OD, JEO; Validation: CYRT, CLT, TC, MM, SB; Visualization: SB; Writing - Original Draft Preparation: SB; Writing - Reviewing and Editing: SB, JEO, CYRT, MM, CYH, OD.

SUPPLEMENTARY MATERIAL

Supplementary material is linked to the online version of the paper at www.jidonline.org, and at https://doi.org/10.1016/j.jid.2021.10.021.

REFERENCES

Alexander E, Hildebrand DG, Kriebs A, Obermayer K, Manz M, Rothfuss O, et al. IκBζ is a regulator of the senescence-associated secretory phenotype in DNA damage- and oncogene-induced senescence. J Cell Sci 2013;126:3738–45.

Bernerd F, Asselineau D. Successive alteration and recovery of epidermal differentiation and morphogenesis after specific UVB-damages in skin reconstructed in vitro. Dev Biol 1997;183:123–38.

Bissett DL, Miyamoto K, Sun P, Li J, Berge CA. Topical niacinamide reduces yellowing, wrinkling, red blotchiness, and hyperpigmented spots in aging facial skin. Int J Cosmet Sci 2004;26:231–8.

Bissett DL, Oblong JE, Berge CA. Niacinamide: a B vitamin that improves aging facial skin appearance. Dermatol Surg 2005;31:860–5.

Chen AC, Martin AJ, Choy B, Fernández-Peñas P, Dalziell RA, McKenzie CA, et al. A phase 3 randomized trial of nicotinamide for skin-cancer chemoprevention. N Engl J Med 2015;373:1618–26.

Chung HT, Joe Y. Antagonistic crosstalk between SIRT1, PARP-1, and -2 in the regulation of chronic inflammation associated with aging and metabolic diseases. Integr Med Res 2014;3:198–203.

Chung JH, Youn SH, Koh WS, Eun HC, Cho KH, Park KC, et al. Ultraviolet B irradiation-enhanced interleukin (IL)-6 production and mRNA expression are mediated by IL-1 alpha in cultured human keratinocytes. J Invest Dermatol 1996;106:715–20.

Coppé JP, Desprez PY, Krtolica A, Campisi J. The senescence-associated secretory phenotype: the dark side of tumor suppression. Annu Rev Pathol 2010;5:99–118.

de Pedro I, Alonso-Lecue P, Sanz-Gómez N, Freije A, Gandarillas A. Sublethal UV irradiation induces squamous differentiation via a p53-independent, DNA damage-mitosis checkpoint. Cell Death Dis 2018;9:1094.

Debacq-Chainiaux F, Leduc C, Verbeke A, Toussaint O. UV, stress and aging. Dermatoendocrinol 2012;4:236–40.

D'Orazio J, Jarrett S, Amaro-Ortiz A, Scott T. UV radiation and the skin. Int J Mol Sci 2013;14:12222–48.

Dreesen O, Chojnowski A, Ong PF, Zhao TY, Common JE, Lunny D, et al. Lamin B1 fluctuations have differential effects on cellular proliferation and senescence. J Cell Biol 2013;200:605–17.

Fania L, Mazzanti C, Campione E, Candi E, Abeni D, Dellambra E. Role of nicotinamide in genomic stability and skin cancer chemoprevention. Int J Mol Sci 2019;20:5946.

Gilchrest BA. Photoaging. J Invest Dermatol 2013;133:E2–6.

Hamanaka RB, Glasauer A, Hoover P, Yang S, Blatt H, Mullen AR, et al. Mitochondrial reactive oxygen species promote epidermal differentiation and hair follicle development. Sci Signal 2013;6:ra8.

Haydont V, Bernard BA, Fortunel NO. Age-related evolutions of the dermis: clinical signs, fibroblast and extracellular matrix dynamics. Mech Ageing Dev 2019;177:150–6.

Hornig-Do HT, von Kleist-Retzow JC, Lanz K, Wickenhauser C, Kudin AP, Kunz WS, et al. Human epidermal keratinocytes accumulate superoxide due to low activity of Mn-SOD, leading to mitochondrial functional impairment. J Invest Dermatol 2007;127:1084–93.

Ke Y, Wang C, Zhang J, Zhong X, Wang R, Zeng X, et al. The role of PARPs in inflammation-and metabolic-related diseases: molecular mechanisms and beyond. Cells 2019;8:1047.

Kim B, Halliday GM, Damian DL. Oral nicotinamide and actinic keratosis: a supplement success story. Curr Probl Dermatol 2015;46:143–9.

Kim HK. Protective effect of garlic on cellular senescence in UVB-exposed HaCaT human keratinocytes. Nutrients 2016;8:464.

Kuehne A, Emmert H, Soehle J, Winnefeld M, Fischer F, Wenck H, et al. Acute activation of oxidative pentose phosphate pathway as first-line response to oxidative stress in human skin cells. Mol Cell 2015;59:359–71.

Lago CU, Nowinski SM, Rundhaug JE, Pfeiffer ME, Kiguchi K, Hirasaka K, et al. Mitochondrial respiratory uncoupling promotes keratinocyte differentiation and blocks skin carcinogenesis. Oncogene 2012;31:4725–31.

Lee JH, An HT, Chung JH, Kim KH, Eun HC, Cho KH. Acute effects of UVB radiation on the proliferation and differentiation of keratinocytes. Photodermatol Photoimmunol Photomed 2002;18:253–61.

Levakov A, Vucković N, Dolai M, Kaćanski MM, Bozanić S. Age-related skin changes. Med Pregl 2012;65:191–5.

Lewis DA, Yi Q, Travers JB, Spandau DF. UVB-induced senescence in human keratinocytes requires a functional insulin-like growth factor-1 receptor and p53. Mol Biol Cell 2008;19:1346–53.

López-Otín C, Blasco MA, Partridge L, Serrano M, Kroemer G. The hallmarks of aging. Cell 2013;153:1194–217.

Luna A, Aladjem MI, Kohn KW. SIRT1/PARP1 crosstalk: connecting DNA damage and metabolism. Genome Integr 2013;4:6.

Oblong JE. The evolving role of the NAD^+/nicotinamide metabolome in skin homeostasis, cellular bioenergetics, and aging. DNA Repair (Amst) 2014;23:59–63.

Osley MA, Tsukuda T, Nickoloff JA. ATP-dependent chromatin remodeling factors and DNA damage repair. Mutat Res 2007;618:65–80.

Quek LS, Grasset N, Jasmen JB, Robinson KS, Bellanger S. Dual role of the anaphase promoting complex/cyclosome in regulating stemness and differentiation in human primary keratinocytes. J Invest Dermatol 2018;138:1851–61.

Quist SR, Wiswedel I, Quist J, Gollnick HP. Kinetic profile of inflammation markers in human skin in vivo following exposure to ultraviolet B indicates synchronic release of cytokines and prostanoids. Acta Derm Venereol 2016;96:910–6.

Rastogi RP, Richa, Kumar A, Tyagi MB, Sinha RP. Molecular mechanisms of ultraviolet radiation-induced DNA damage and repair. J Nucleic Acids 2010;2010:592980.

Rheinwald JG, Green H. Serial cultivation of strains of human epidermal keratinocytes: the formation of keratinizing colonies from single cells. Cell 1975;6:331–43.

Rünger TM, Farahvash B, Hatvani Z, Rees A. Comparison of DNA damage responses following equimutagenic doses of UVA and UVB: a less effective cell cycle arrest with UVA may render UVA-induced pyrimidine dimers more mutagenic than UVB-induced ones. Photochem Photobiol Sci 2012;11:207–15.

Schuch AP, Moreno NC, Schuch NJ, Menck CFM, Garcia CCM. Sunlight damage to cellular DNA: focus on oxidatively generated lesions. Free Radic Biol Med 2017;107:110–24.

Sesto A, Navarro M, Burslem F, Jorcano JL. Analysis of the ultraviolet B response in primary human keratinocytes using oligonucleotide microarrays. Proc Natl Acad Sci USA 2002;99:2965–70.

Shin JW, Kwon SH, Choi JY, Na JI, Huh CH, Choi HR, et al. Molecular mechanisms of dermal aging and antiaging approaches. Int J Mol Sci 2019;20:2126.

Simon M, Green H. Enzymatic cross-linking of involucrin and other proteins by keratinocyte particulates in vitro. Cell 1985;40:677–83.

Surjana D, Halliday GM, Damian DL. Role of nicotinamide in DNA damage, mutagenesis, and DNA repair. J Nucleic Acids 2010;2010:157591.

Tagami H. Functional characteristics of the stratum corneum in photoaged skin in comparison with those found in intrinsic aging. Arch Dermatol Res 2008;300(Suppl. 1):S1–6.

Tamiji S, Beauvillain JC, Mortier L, Jouy N, Tual M, Delaporte E, et al. Induction of apoptosis-like mitochondrial impairment triggers antioxidant and Bcl-2-dependent keratinocyte differentiation. J Invest Dermatol 2005;125:647–58.

Tan CL, Chin T, Tan CYR, Rovito HA, Quek LS, Oblong JE, et al. Nicotinamide metabolism modulates the proliferation/differentiation balance and senescence of human primary keratinocytes. J Invest Dermatol 2019;139:1638–47.e3.

Thierry F, Benotmane MA, Demeret C, Mori M, Teissier S, Desaintes C. A genomic approach reveals a novel mitotic pathway in papillomavirus carcinogenesis. Cancer Res 2004;64:895–903.

Wang AS, Ong PF, Chojnowski A, Clavel C, Dreesen O. Loss of lamin B1 is a biomarker to quantify cellular senescence in photoaged skin. Sci Rep 2017;7:15678.

Wiley CD, Velarde MC, Lecot P, Liu S, Sarnoski EA, Freund A, et al. Mitochondrial dysfunction induces senescence with a distinct secretory phenotype. Cell Metab 2016;23:303–14.

Yaar M, Gilchrest BA. Photoageing: mechanism, prevention and therapy. Br J Dermatol 2007;157:874–87.

SUPPLEMENTARY MATERIALS AND METHODS

Senescence-associated β-galactosidase assays

Human primary keratinocytes were cultured on glass coverslips and analyzed for senescence-associated β-galactosidase activity 5 days after treatment with UVB or hydrogen peroxide using the Senescence β-Galactosidase Staining Kit (9860, Cell Signaling Technology, Danvers, MA). Images were captured using an AxioImager Z1 (Zeiss, Oberkochen, Germany) microscope using a ×20 plan apochromatic objective lens. Senescence-associated β-galactosidase–positive cells were counted manually.

SenTraGor (GL13) staining

Paraffin-embedded tissue sections were dewaxed and rehydrated, followed by antigen retrieval and treatment with hydrogen peroxide and goat serum, as described in the section "Immunohistochemistry analysis of 3D organotypic sections" in the main manuscript. Sections were then washed with PBS/0.05% Tween 20, 50% ethanol, and 70% ethanol (5 minutes per wash). SenTraGor reagent (Lab Supplies Scientific — P.Galanis, Athens, Greece) was prepared according to the manufacturer's instructions, and one drop was placed on each section using a 1-ml syringe attached to a 13 mm/0.22 μM membrane filter. A coverslip was then placed on top, and the section was incubated at 37 °C for 10 minutes. Excess SenTraGor reagent was removed using Kimwipes dipped in ethanol, followed by four 50% ethanol washes (5 minutes per wash). Sections were washed with PBS/0.05% Tween 20 for 5 minutes and incubated overnight with mouse anti-biotin (Ab201341 [Hyb-8], 1:500, Abcam, Cambridge, United Kingdom). They were then washed again with water and PBS/0.05% Tween 20 before incubation for 30 minutes with EnVision+ System-HRP Labelled Polymer anti-mouse antibody (K4001, Dako, Carpinteria, CA). Sections were then washed with water and PBS/0.05% Tween 20 before incubation with Liquid DAB+ Substrate Chromogen System (K3468, Dako) for 2 minutes. After washing with water, they were mounted using Hydromount (Electron Microscopy Sciences, Hatfield, PA).

Algorithm used for quantification of Lamin B1

The following algorithm was used for Lamin B1 quantification:

```
//John Lim, AMP, 16 May 2019
//Measure centroid of nuclei
//Ecad mean intensity, nuclei y-center
//Lamin threshold mean intensity, threshold area faction
//Reject those negative distance
nuclei_ch = 1;
nuclei_modifier = 1; //threshold modifier
minSize = 2; //nuclei minimum area
maxSize = 300; //nuclei maximum area
K10_ch = 2;
K10_bg = 191;
Lamin_ch = 3;
Lamin_bg = 263;
reset_to_pixel = false; //if true, reset unit to pixel, if false fellow calibration below
calibration = 0.16125; //distance per pixel
pixel_unit = "micro";

substrate_ch = 3;
minS = 1000; maxS = 5000;

//function
function data_table(a, b, c, d, e, f){
title1="Data_Table";
title2="["+title1+"]";
if (isOpen(title1)){
    print(title2, a+"\t"+b+"\t"+c+"\t"+d+"\t"+e+"\
    t"+f);
}
else{run("Table...", "name="+title2+" width=800
    height=600");
print(title2, "\\Headings:Label\tX\tY\tArea\tK10_MeanIn
    tensity\tLaminB1_Threshold_Mean_Intensity");
print(title2, a+"\t"+b+"\t"+c+"\t"+d+"\t"+e+"\t"+f);
}
}

//table
Table.create("Data_Table");
Table.showRowNumbers(true); //Enable or disable
display of row numbers.
//Table.set(columnName, rowIndex, value);
//Table.update;
//parameters
requires("1.52a"); //check ImageJ version
setOption("BlackBackground", true);
roiManager("reset");
if(reset_to_pixel == true){
run("Set Scale...", "distance=0");

}
if(reset_to_pixel == false){
run("Set Scale...", "distance=1 known=calibration unit="
    +pixel_unit);

}

//run("Set Measurements...", "area mean centroid display
redirect=None decimal=3");
setBatchMode(true);
id0 = getImageID();

title0 = getTitle();
getDimensions(width, height, channels, slices, frames);
//Substrate
selectImage(id0);
run("Duplicate...", "title=substrate duplicate channels=substrate_ch");
//run("Gaussian Blur...", "sigma=2");
run("Subtract Background...", "rolling=50");
setAutoThreshold("Default dark");
run("Analyze Particles...", "size="+minS+"-"+maxS+"
circularity=0.00-1.00 add");
sCount = roiManager("count");
if(sCount != 1){
print("More than one or Zero substrate was detected
    "+title0);
}

if(sCount == 1){
roiManager("select", 0);
```

```
 List.setMeasurements();
 substrate_y = List.getValue("Y");
 roiManager("reset")
}
//Find nuclei ROIs
selectImage(id0);
run("Duplicate...", "title=nuclei duplicate channels=nuclei_ch");
id1 = getImageID();
title1 = getTitle();
run("Gaussian Blur...", "sigma=2 slice");
run("Subtract Background...", "rolling=50");
//run("Unsharp Mask...", "radius=1 mask=0.60");
//run("Enhance Local Contrast (CLAHE)", "blocksize=127
histogram=256 maximum=3 mask=*None* fast_(less_
accurate)");
setAutoThreshold("Default dark");
getThreshold(n1, n2);
setThreshold(nuclei_modifier*n1, n2);
maxSizeE = maxSize * 10;
run("Analyze Particles...", "size="+minSize+"-"+maxSizeE+"
circularity=0.10-1.00 show=Masks");
run("Grays");
run("Watershed");
run("Analyze Particles...", "size="+minSize+"-"+maxSize+"
circularity=0.45-1.00 show=Nothing exclude add");
id2 = getImageID();
selectImage(id1); close();
selectImage(id2); close();
nROI = roiManager("count");
if(nROI > 0){
 for (i = 0; i < nROI; i++) {
    selectImage(id0);
    roiManager("select", i)
    roiName = Roi.getName;
    Stack.setChannel(K10_ch);
    List.setMeasurements();
    x = List.getValue("X");
    y = List.getValue("Y");
    area = List.getValue("Area");
    mean1 = List.getValue("Mean");
    mean1 = mean1 - K10_bg;
    Stack.setChannel(Lamin_ch);
    setAutoThreshold("Default dark");
    getThreshold(lower, upper);
    setThreshold(lower, upper);
    List.setMeasurements("limit");
    mean2 = List.getValue("Mean");
    mean2 = mean2 - Lamin_bg;
    //data_table(title0+"_"+roiName, x, y, area, mean1,
     mean2);
    ydistanceS = substrate_y - y;
    if(sCount == 1 && ydistanceS > 1){
       nrow = Table.size; //print(nrow);
       Table.set("Label", nrow, title0+"_"+roiName);
       Table.set("X", nrow, x); Table.set("Y", nrow, y);
       Table.set("Area", nrow, area);
       Table.set("K10_MeanIntensity", nrow, mean1); Table.-
       set("Lamin_Threshold_MeanIntensity", nrow, mean2);
       Table.set("ydistanceS", nrow, ydistanceS);
       Table.update;
 }
 }

}
roiManager("Deselect");
run("Select None");
resetThreshold();
selectImage(id0);
run("Remove Overlay");
if(sCount == 1){
 Stack.setChannel(nuclei_ch);
 if(reset_to_pixel == false){
 substrate_y_pixel = substrate_y / calibration;
 }
 else{
 substrate_y_pixel = substrate_y;
 }
 //Overlay.drawLine(0, substrate_y_pixel, width-1, substrate_y_pixel);
 //Overlay.show;
 makeLine(0, substrate_y_pixel, width-1, substrate_y_pixel);
 roiManager("Add");
 roiManager("Remove Channel Info");
 roiManager("Remove Slice Info");
 roiManager("Remove Frame Info");

}roiManager("Deselect");
roiManager("Show All without labels");
print("Done");
```

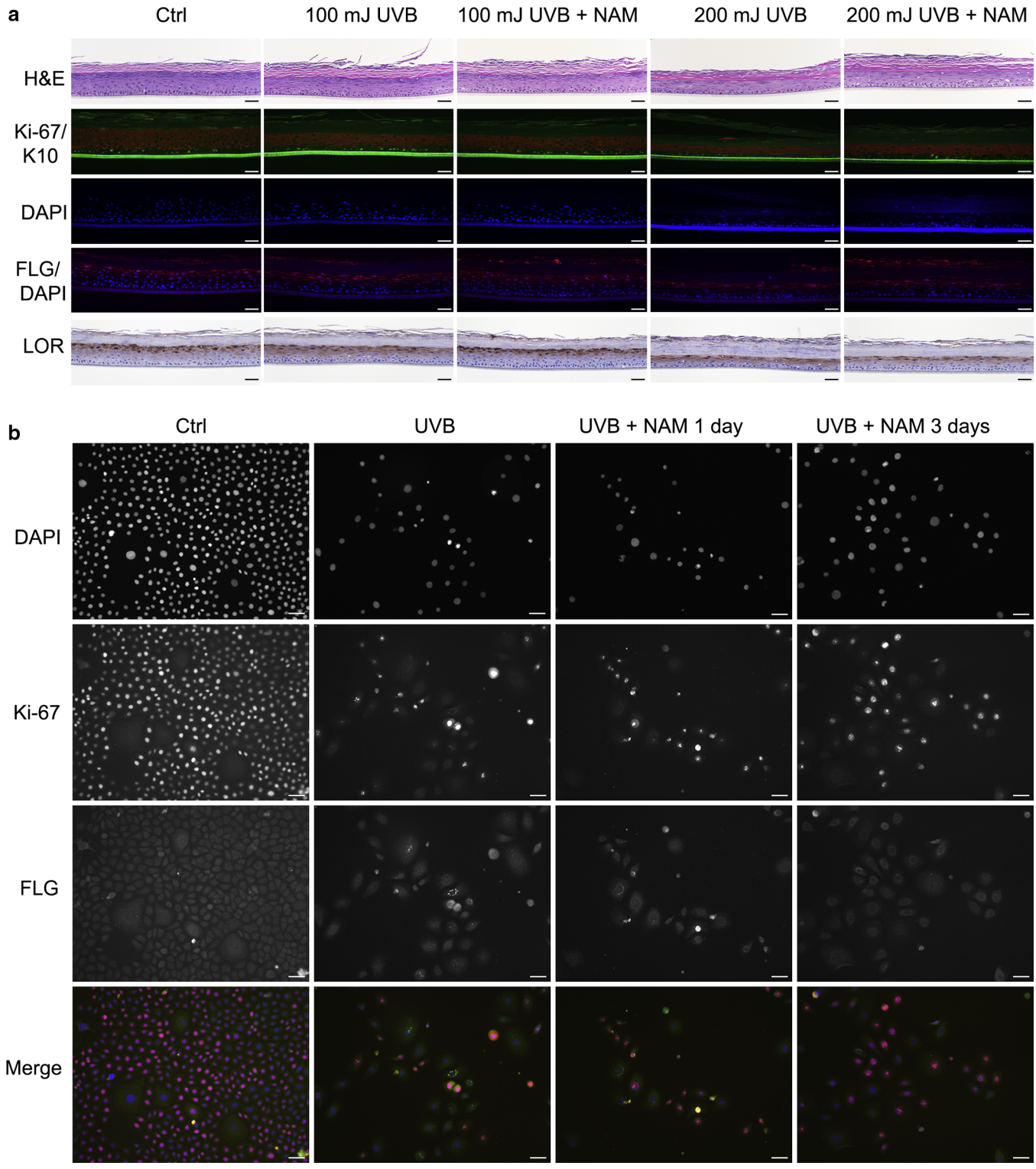

Supplementary Figure S1. NAM prevents premature late differentiation induced by UVB in both 3D organotypics and 2D cultures of HPKs. (**a**) HPKs were grown to a full-thickness epithelium before irradiation with 100 or 200 mJ/cm^2 UVB ± NAM (single dose) and harvested on day 6 after treatment. H&E, immunohistochemical, and immunofluorescence staining were performed. Bar = 50 μm. (**b**) Immunofluorescence analyses of proliferation and differentiation markers on day 3 after HPK treatment with UVB ± NAM for 1 day or 3 days in 2D. Bar = 50 μm. The channels are separated, compared with those in Figure 1 in which they are merged. 2D, two-dimensional; 3D, three-dimensional; Ctrl, untreated control cell; FLG, filaggrin; HPK, human primary keratinocyte; K10, keratin 10; LOR, loricrin; NAM, nicotinamide.

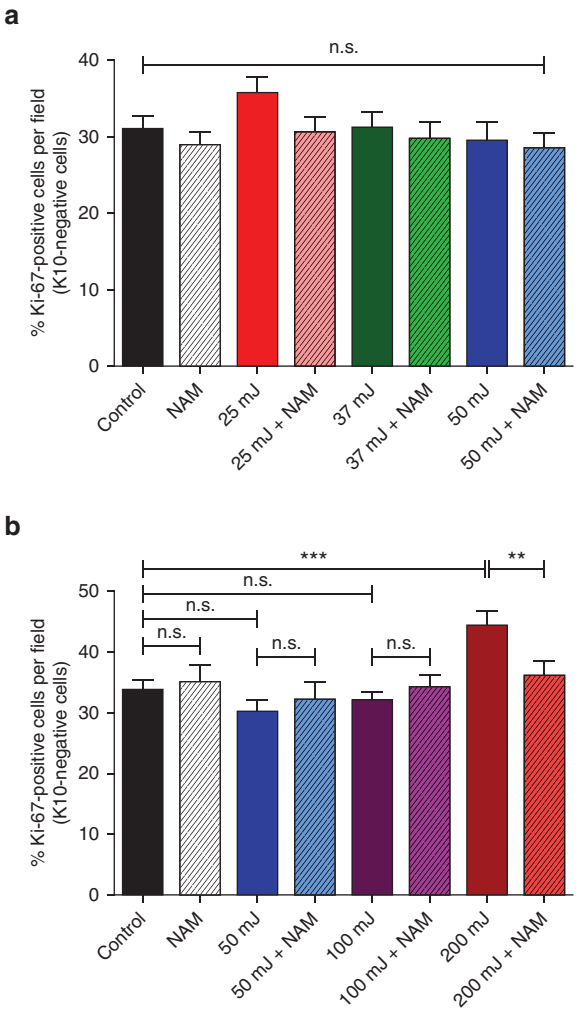

Supplementary Figure S2. Analyses of proliferation in 3D organotypics after low or high doses of UVB irradiation. (**a**) Percentage of Ki-67–positive cells in the basal layer (low UVB doses). A total of 10–17 fields per condition were analyzed (from triplicates). (**b**) Percentage of Ki-67–positive cells in the basal layer (high UVB doses). A total of 21–34 fields per condition were analyzed (from triplicates). In both cases, statistical analyses were performed with unpaired *t*-tests, and the data represent the means ± SEM. *P*-values < 0.05 indicate statistical significance (**$P < 0.01$; ***$P < 0.001$). 3D, three-dimensional; NAM, nicotinamide; n.s., not significant.

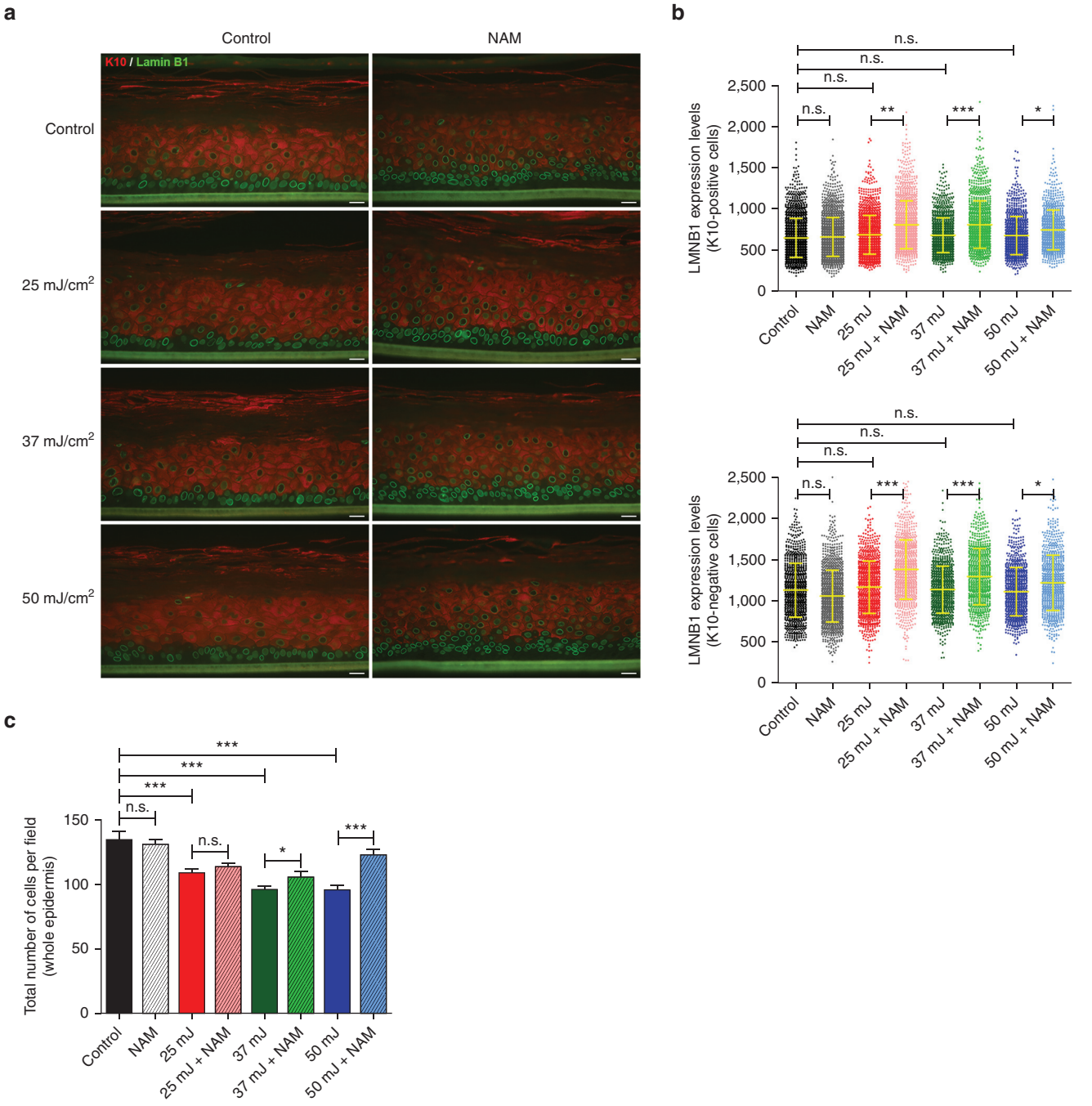

Supplementary Figure S3. Analyses of senescence in 3D organotypic models after low doses of UVB irradiation. (**a**) HPKs were grown to a full-thickness epithelium before irradiation with 25, 37, or 50 mJ/cm^2 UVB (single dose) and harvested on day 6 after treatment. Immunofluorescence analyses of the LMB1 senescence marker (green) and the K10 differentiation marker (red). Bar = 20 μm. (**b**) LMNB1 levels per cell in basal (lower panel) and upper (upper panel) layers were quantified using a custom algorithm in ImageJ, version 1.52o. Each dot represents one cell. A total of 800−1,800 cells per condition (from triplicates) were analyzed depending on samples. Statistical analyses: unpaired *t*-tests. Data represent the means ± SD. (**c**) Total number of cells per field (according to DAPI) under each condition. A total of 17−24 fields per condition were analyzed (from triplicates). Statistical analyses: unpaired *t*-tests. Data represent the means ± SEM. For all panels, *P*-values < 0.05 indicate statistical significance (*$P < 0.05$; **$P < 0.01$; ***$P < 0.001$). 3D, three-dimensional; HPK, human primary keratinocyte; K10, keratin 10; LMNB1, lamin B1; NAM, nicotinamide; n.s., not significant.

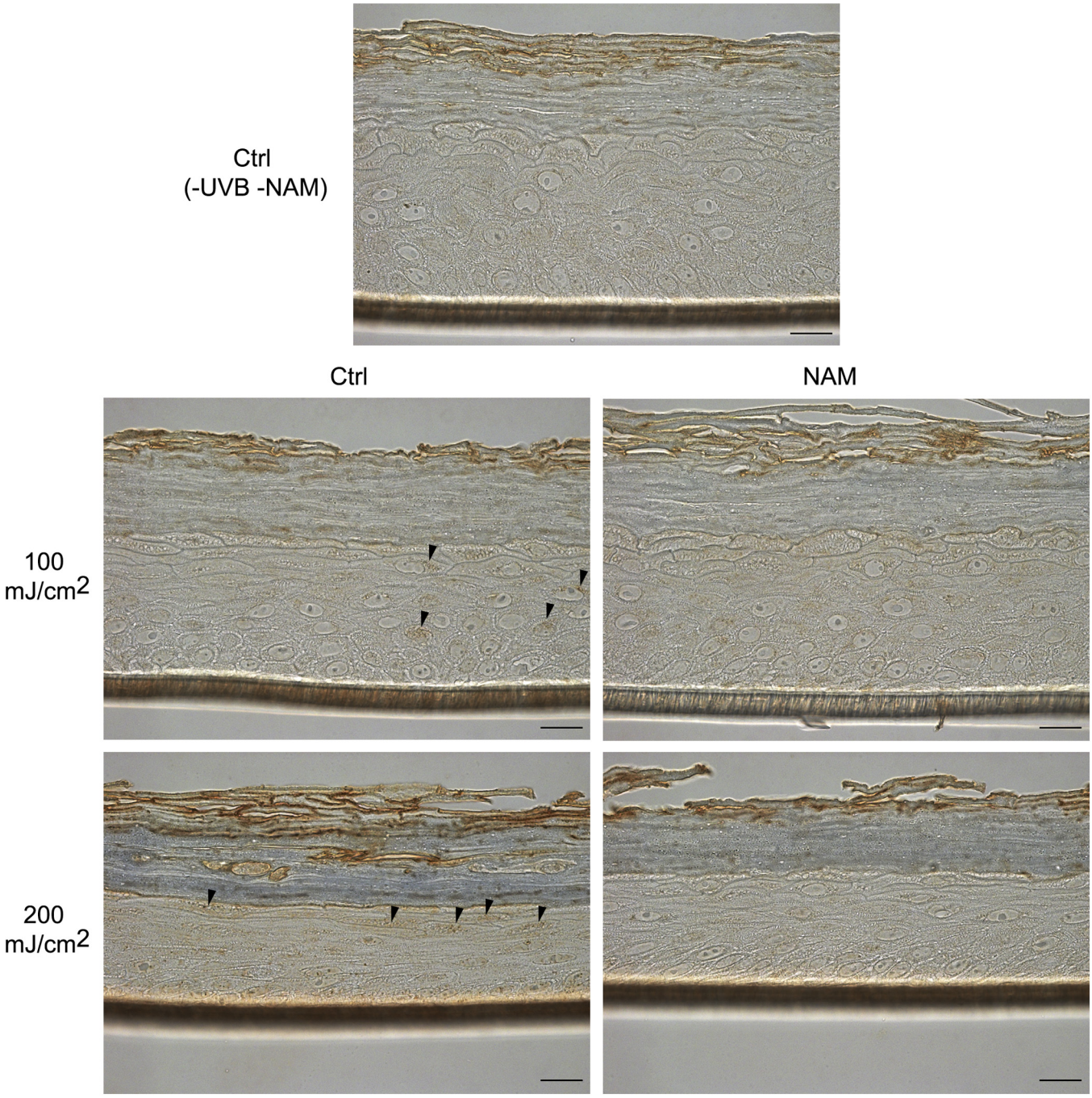

Supplementary Figure S4. Lipofuscin detection in 3D organotypic sections after UVB irradiation. The 3D organotypic sections treated as indicated were stained with SenTraGor (GL13) on day 6 after UVB irradiation (100 or 200 mJ/cm^2). Arrows indicate cells presenting granules of lipofuscin. Bar = 20 μm. 3D, three-dimensional; Ctrl, untreated control cell; NAM, nicotinamide.

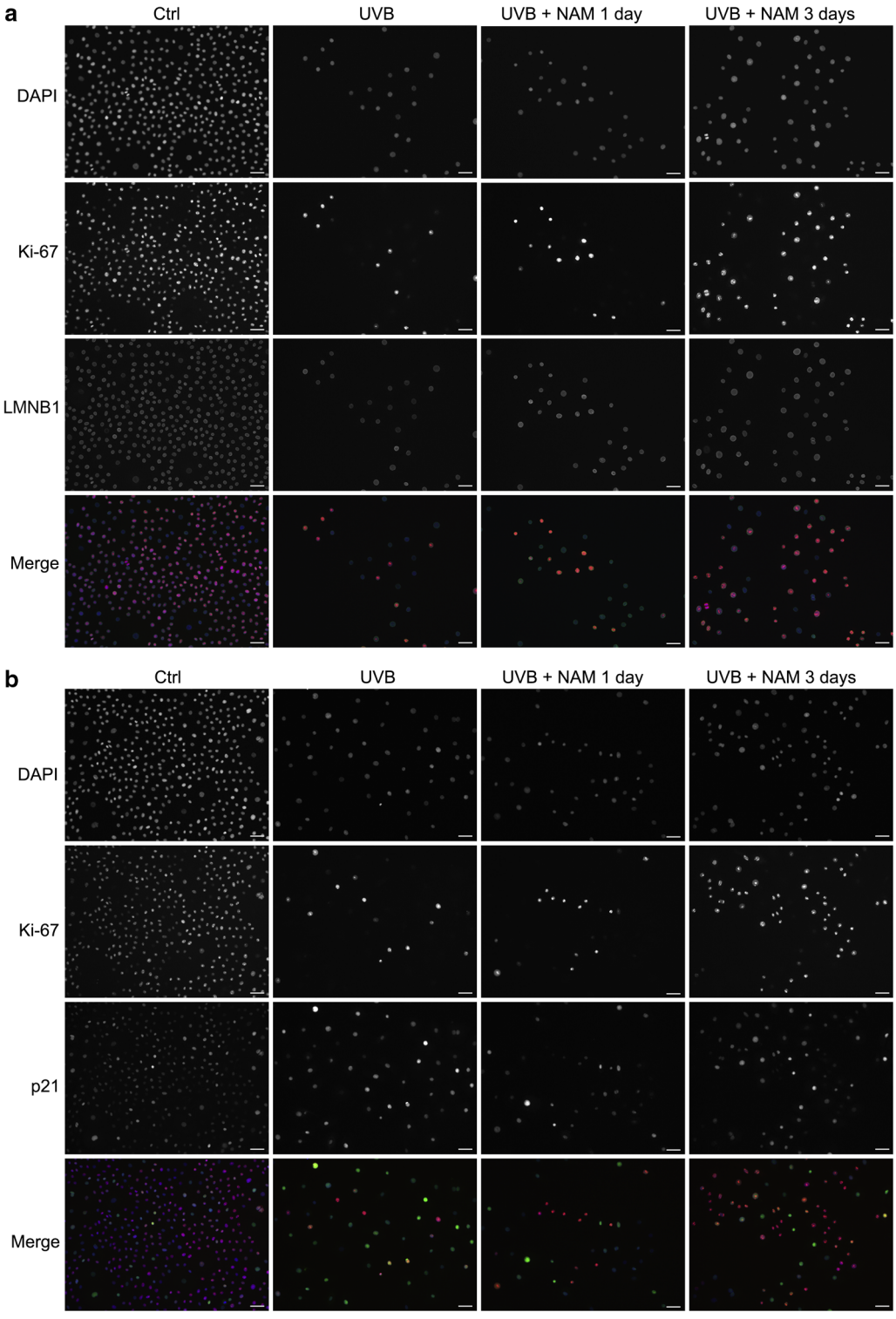

Supplementary Figure S5. Analyses of senescence and proliferation in 2D models after UVB irradiation. (**a**) Immunofluorescence analyses of the LMNB1 senescence marker on day 3 after treatment of HPKs with UVB (25 mJ/cm^2) ± NAM for 1 day or 3 days. Bar = 50 μm. (**b**) Immunofluorescence analyses of the p21 senescence marker under the same conditions as in **a**. Bar = 50 μm. For both **a** and **b**, the channels are separated, compared with those in Figure 3 in which they are merged. 2D, two-dimensional; Ctrl, untreated control cell; HPK, human primary keratinocyte; LMNB, lamin B1; NAM, nicotinamide.

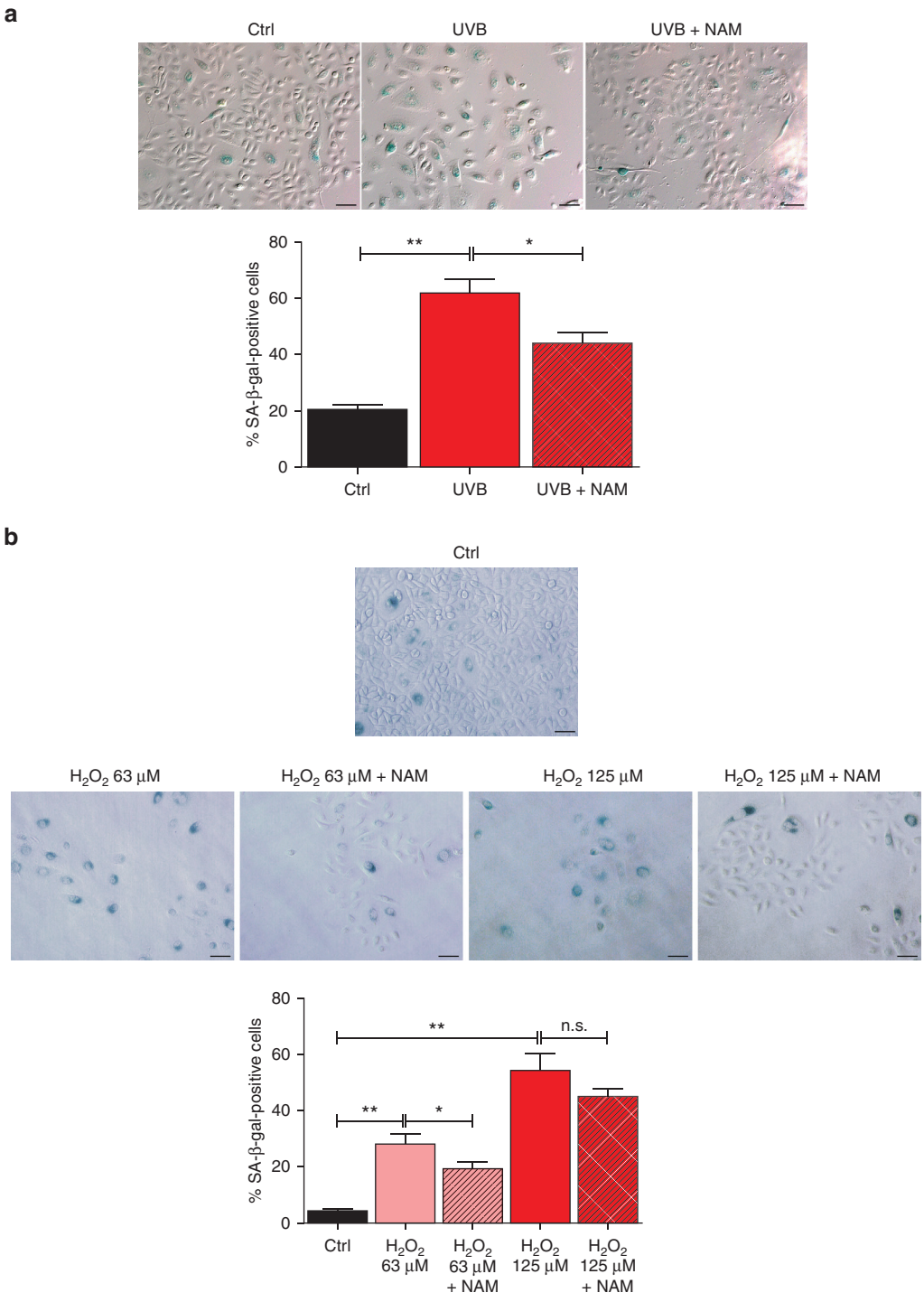

Supplementary Figure S6. NAM prevents senescence induced by both UVB irradiation and H_2O_2 treatment in 2D cultures of HPKs. (**a**) HPKs grown in 2D cultures were treated with UVB 25 mJ/cm^2 and analyzed for SA-β-gal expression 5 days after treatment. Upper panel: phase-contrast images showing SA-β-gal in blue. Bar = 50 μm. Lower panel: quantification of SA-β-gal–positive cells in the indicated populations; n ≥ 300 cells for each condition. (**b**) HPKs grown in 2D cultures were treated with H_2O_2, and the experiment was performed as in **a**. Upper panel: phase-contrast images showing SA-β-gal staining in blue. Bar = 50 μm. Lower panel: quantification of SA-β-gal–positive cells in the indicated populations; n ≥ 300 cells for each condition. In all cases, statistical analyses: one-way ANOVA; n = 3 for **a** or 4 for **b**. Data represent the means ± SEM. *P*-values < 0.05 indicate statistical significance (*$P < 0.05$; **$P < 0.01$). 2D, two-dimensional; Ctrl, untreated control cell; H_2O_2, hydrogen peroxide; HPK, human primary keratinocyte; NAM, nicotinamide; n.s., not significant; SA-β-gal, senescence-associated β-galactosidase.

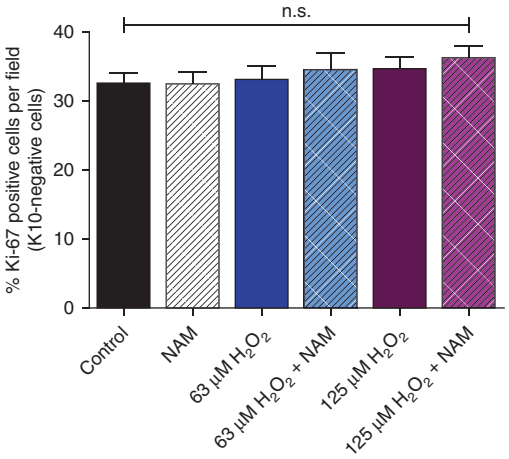

Supplementary Figure S7. Analyses of Ki-67 expression in 2D models of HPKs after treatment with H_2O_2. HPKs were grown to full-thickness epithelia before treatment with H_2O_2 (63 and 125 μM) and harvested on day 6 after treatment. The graph shows the percentage of Ki-67–positive cells in the basal layer. A total of 11–20 fields per condition were analyzed (from triplicates). Statistical analyses: unpaired *t*-tests. Data represent the means ± SEM. *P*-values < 0.05 indicate statistical significance. 2D, two-dimensional; H_2O_2, hydrogen peroxide; HPK, human primary keratinocyte; K10, keratin 10; NAM, nicotinamide; n.s., not significant.

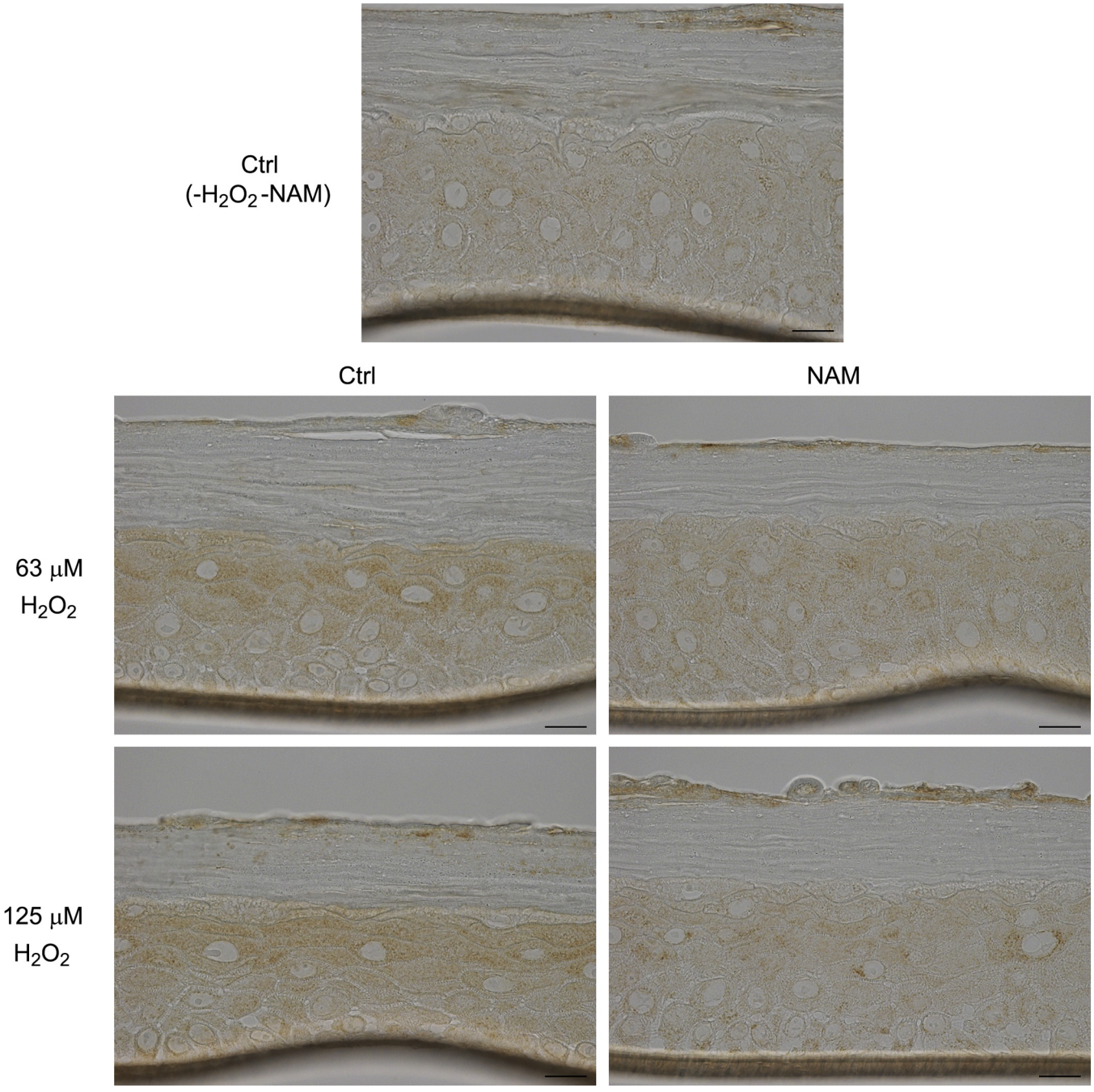

Supplementary Figure S8. Lipofuscin detection in 3D organotypic sections after H_2O_2 treatment (63 or 125 μM). The 3D organotypic sections treated as indicated were stained with SenTraGor (GL13) on day 6 after H_2O_2 treatment. Bar = 20 μm. 3D, three-dimensional; Ctrl, untreated control cell; H_2O_2, hydrogen peroxide; NAM, nicotinamide.

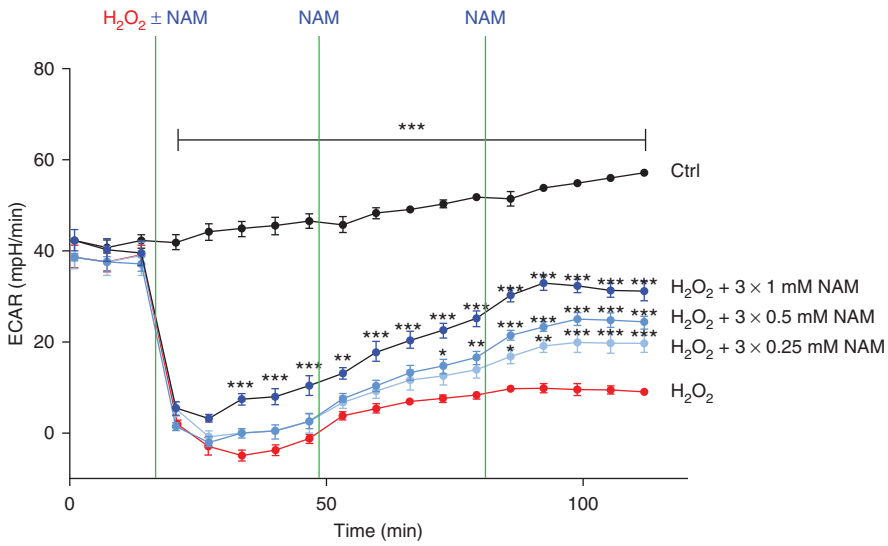

Supplementary Figure S9. Dose-dependent rescue of energy metabolism by NAM after H_2O_2 treatment. Basal ECAR levels after treatment with $H_2O_2 \pm$ NAM (one injection of H_2O_2, three injections of NAM). Statistical analyses: two-way ANOVA; n = 3. Data represent the means ± SEM. *P*-values < 0.05 indicate statistical significance (*$P < 0.05$; **$P < 0.01$; ***$P < 0.001$). ECAR, extracellular acidification rate; H_2O_2, hydrogen peroxide; min, minute; NAM, nicotinamide; n.s., not significant.

Supplementary Table S1. Primer Sequences for RT-qPCR

Primer Name	Sequence (5′−3′)
TBP	F: CGTCCCAGCAGGCAACAC R: TTGTGAGAGTCTGTGAGTGGAAGAG
IVL	F: CCATCAGGAGCAAATGAAACAG R: GCTCGACAGGCACCTTCTG
FLG	F: GTGTTAGTTACAATTCCAATCCTGTTG R: ATACGTTGCATAATACCTTGGATGATC
LMNB1	F: CGCTTGGTAGAGGTGGATTCTG R: CCTCACTTGGGCATCATGTTG
p21	F: GCGACTGTGATGCGCTAATG R: CGGTGACAAAGTCGAAGTTCC

Abbreviations: F, forward; FLG, filaggrin; IVL, involucrin; LMNB1, lamin B1; R, reverse; TBP, TATA-binding protein.

Supplementary Table S2. Primary Antibodies for 2D Immunofluorescence, Western Blotting, 3D Immunohistochemistry/Fluorescence, and ELISA

Primary Antibody	Dilution	Source (Catalog Number; Supplier)
2D immunofluorescence		
Ki-67	1:500	ab15580; Abcam, Cambridge, UK
LMNB1	1:500	NBP2-48966, Novus Biologicals, Littleton, CO
p21	1:500	Waf1/Cip1 (12D1), #2947; Cell Signaling Technology, Danvers, MA
CPD (TDM-2)	1:1,500	CAC-NM-DND-001; Cosmo Bio, Tokyo, Japan
Western blotting		
IVL	1:500	Novocastra NCL-INV; Leica Biosystems, Richmond, IL
LMNB1	1:10,000	ab16048; Abcam, Cambridge, UK
Actin	1:1,000	A2066; Sigma-Aldrich, St. Louis, MO
3D immunohistochemistry/fluorescence		
K10 (mouse)	1:200	DE-K10, M7002, Dako, Agilent, Santa, Clara, CA
K10 (rabbit)	1:200	EP16071HCY, ab76318, Abcam, Cambridge, UK
FLG	1:200	FLG/1561, ab218395; Abcam, Cambridge, UK
LOR	1:500	EPR7148(2)(B), ab176322; Abcam, Cambridge, UK
Ki-67	1:200	MIB-1; M7240; Dako, Agilent, Santa Clara, CA
LMNB1	1:100	NBP2-48966, Novus Biologicals, Littleton, CO
ELISA		
IL-6	—	ab100572, ab229434; Abcam, Cambridge, UK
IL-8	—	ab46032, ab229402; Abcam, Cambridge, UK

Abbreviations: 2D, two-dimensional; 3D, three-dimensional; CPD, cyclobutane pyrimidine dimer; FLG, filaggrin; IVL, involucrin; K10, keratin 10; LMNB1, lamin B1; LOR, loricrin; UK, United Kingdom.